Supporting Information

Porous Metal–Organic Polyhedral Frameworks with Optimal Molecular Dynamics and Pore Geometry for Methane Storage

Yong Yan,[1†] Daniil I. Kolokolov,[2,3†] Ivan da Silva,[4†] Alexander G. Stepanov,[2,3] Alexander J. Blake,[5] Anne Dailly,[6] Pascal Manuel,[4] Chiu C. Tang,[7] Sihai Yang[1]* and Martin Schröder[1,8]*

1. School of Chemistry, University of Manchester, Oxford Road, Manchester, M13 9PL, United Kingdom. Sihai.Yang@manchester.ac.uk; M.Schroder@manchester.ac.uk

2. Boreskov Institute of Catalysis, Siberian Branch of Russian Academy of Sciences, Prospekt Akademika Lavrentieva 5, Novosibirsk 630090, Russia.

3. Novosibirsk State University, Pirogova Street 2, Novosibirsk 630090, Russia.

4. ISIS facility, Science and Technology Facilities Council (STFC), Rutherford Appleton Laboratory, Didcot, OX11 0QX, United Kingdom.

5. School of Chemistry, University of Nottingham, University Park, Nottingham, NG7 2RD, United Kingdom.

6. Chemical and Environmental Sciences Laboratory, General Motors Corporation, Warren, Michigan 48090, United States.

7. Diamond Light Source, Harwell Science and Innovation Campus, Didcot, Oxfordshire, OX11 0DE, United Kingdom.

8. Nikolaev Institute of Inorganic Chemistry, Siberian Branch of the Russian Academy of Sciences, 3 Acad. Lavrentiev Ave., Novosibirsk, 630090, Russia.

[†]These authors contributed equally to this work.

Table of Contents

Section S1. Synthesis of H_6BTAT

General Information. Commercially available reagents were used without further purification unless stated otherwise. Nuclear magnetic resonance (NMR) spectra were recorded on a Bruker 300 MHz NMR spectrometer at working frequencies of 300.13 (^{1}H) and 75.47 (^{13}C) MHz. Fourier transform infrared (FTIR) spectra were performed on a Nicolet iS5 spectrometer using the attenuated total reflectance (ATR) mode. Elemental analyses were carried out on a CE-440 elemental analyser.

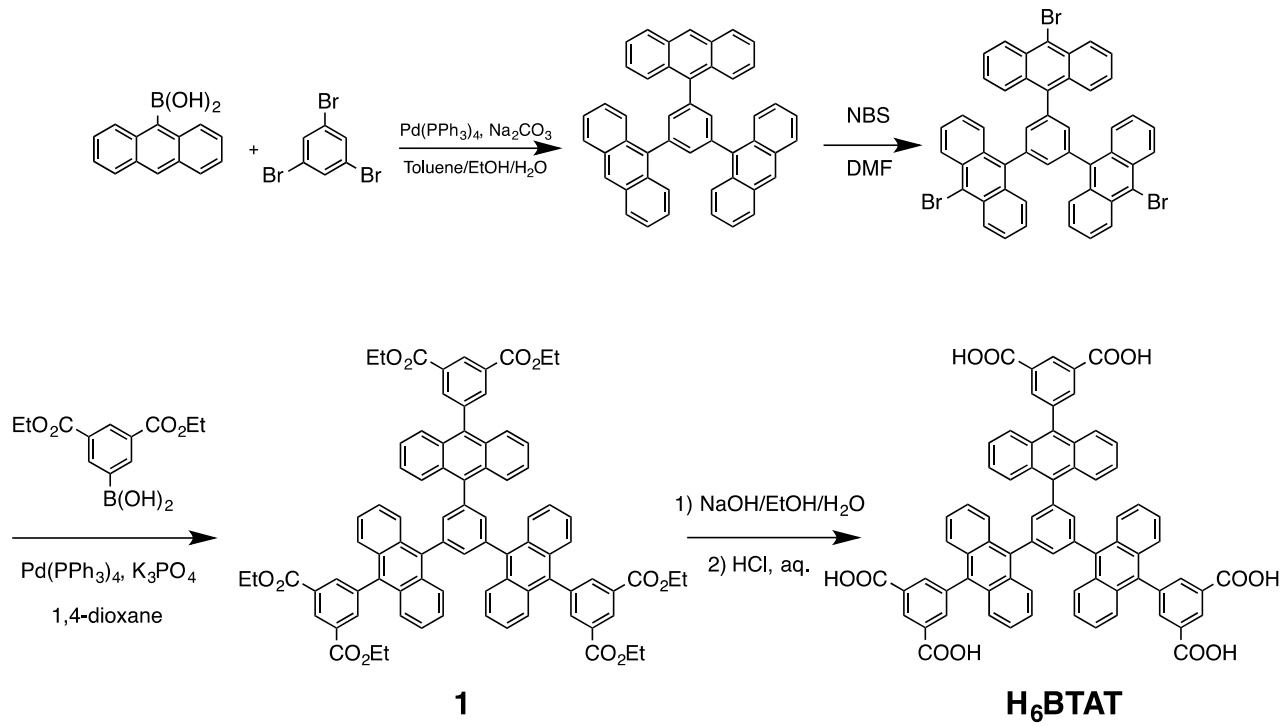

Scheme S1. Synthesis of the hexacarboxylate linker H_6BTAT.

Synthesis of Hexaethyl-5,5',5''-(benzene-1,3,5-triyltris(anthracene-10,9-diyl))triisophthalate (1). 1,3,5-Tris(10-bromoanthracen-9-yl)benzene[1] (2.0 g, 2.4 mmol), diethylisophthalate-5-boronic acid (2.3 g, 8.5 mmol), and K_3PO_4 (4.5 g, 21.2 mmol) were mixed with 1,4-dioxane (100 mL), and the mixture de-aerated by using dry argon for 20 min. [$Pd(PPh_3)_4$] (152 mg, 0.13 mmol) was added to the stirred reaction mixture under Ar, and the mixture heated at 90 °C for 48 h under a constant flow of Ar, after which 1,4-dioxane was removed under vacuum. The resultant solid was treated with a mixture of water (100 mL) and $CHCl_3$ (100 mL). The organic layer was washed with NH_4Cl solution (3 × 50 mL) and brine, and then dried over $MgSO_4$. The solvent was removed under vacuum and the residue purified by column chromatography using ethyl acetate/hexane (1:3) as eluent to yield pure ester (2.6 g, 85% yield).

Synthesis of 5,5',5''-(benzene-1,3,5-triyltris(anthracene-10,9-diyl))triisophthalic acid (H_6BTAT). Compound **1** (2.6 g, 2 mmol) was suspended in a mixture of THF (50 mL) and EtOH (50 mL), to which was added an aqueous solution of NaOH (2 M, 50 mL). The mixture was stirred under reflux overnight and THF and EtOH were removed under vacuum. Dilute HCl (2M) was added to the remaining aqueous solution until the solution was at pH = 3. The precipitate was collected by filtration, washed with water and EtOH, and dried to give H_6BTAT as a light yellow solid (2.2 g, 96% yield). ^{1}H NMR (300 MHz, DMSO-d_6, ppm): δ 13.43 (s, 6 H), 8.7 (t, J = 1.7 Hz, 3 H), 8.31 (d, J = 8.7 Hz, 6 H), 7.84 (s, 3 H), 7.75–7.71 (m, 6 H), 7.58–7.50 (m, 12 H). ^{13}C NMR (75 MHz, DMSO-d_6, ppm): 166.91, 139.4, 139.34, 136.89, 135.99, 135.18, 132.5, 129.99, 129.86, 129.75, 126.97, 126.74, 126.59. HRMS (ESI): *m/z* calcd for $C_{72}H_{41}O_{12}$: 1098.2676 ([M - H]$^-$); found 1098.2460.

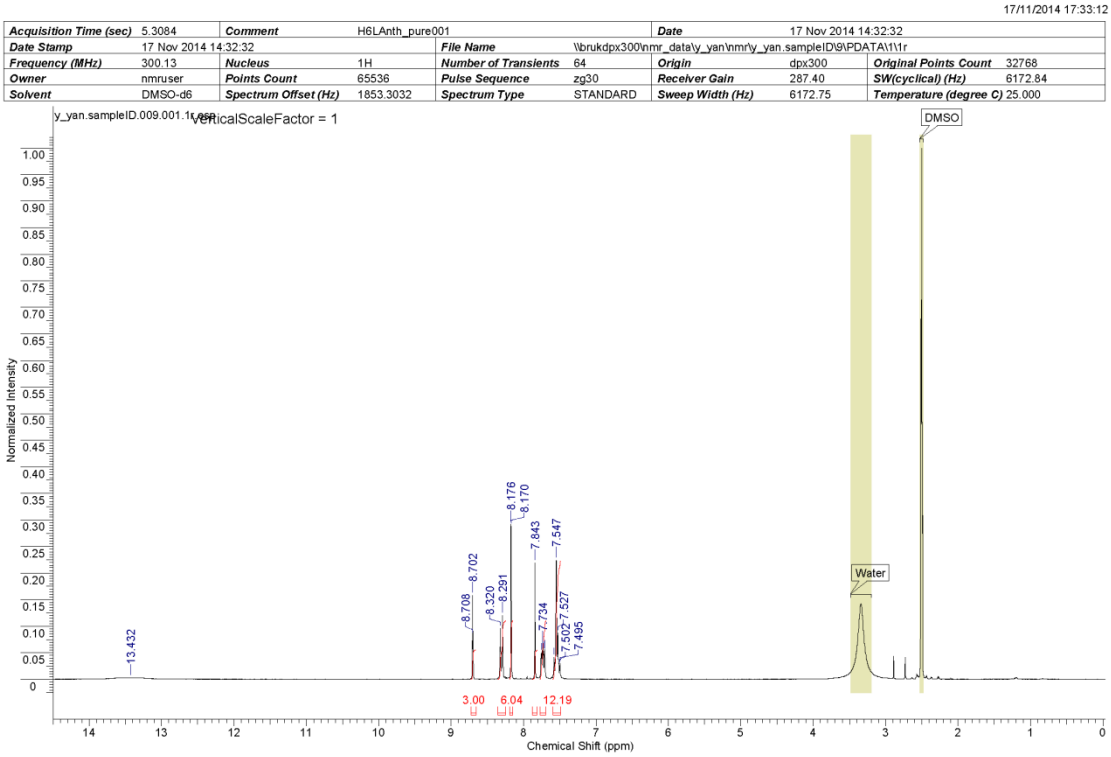

(a)

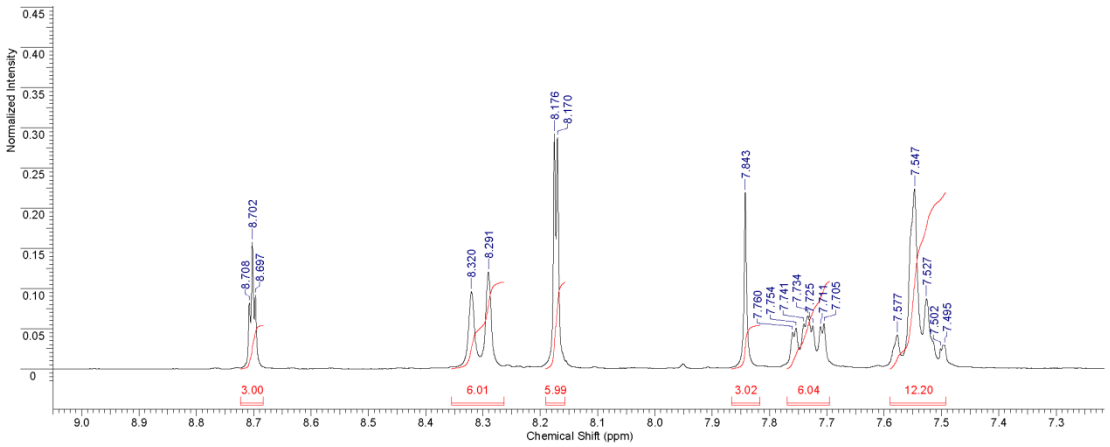

(b)

Figure S1. (a) ^{1}H NMR spectrum of 5,5',5"-(benzene-1,3,5-triyltris(anthracene-10,9-diyl))triisophthalic acid (H_6BTAT) in DMSO-d_6. (b) The ^{1}H NMR spectrum in the region 9.0–7.3 ppm. Note that the compound recrystallized from DMF/H_2O still contained a small amount of DMF (~5 mol%) after drying.

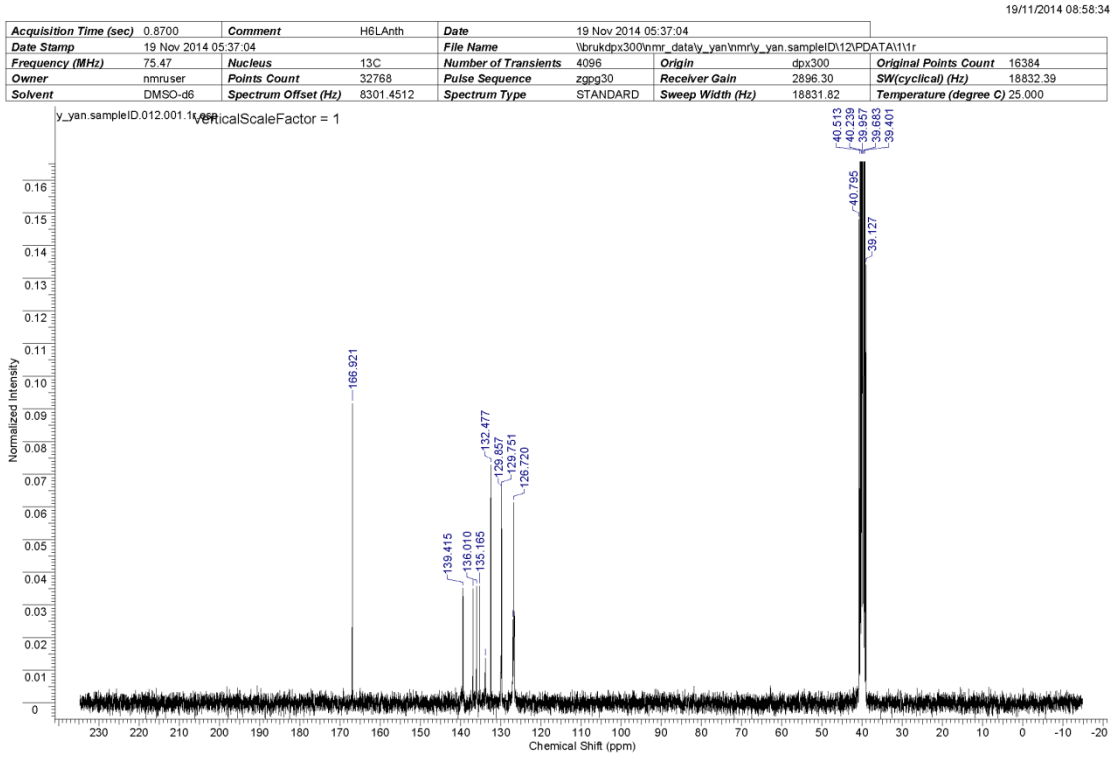

(a)

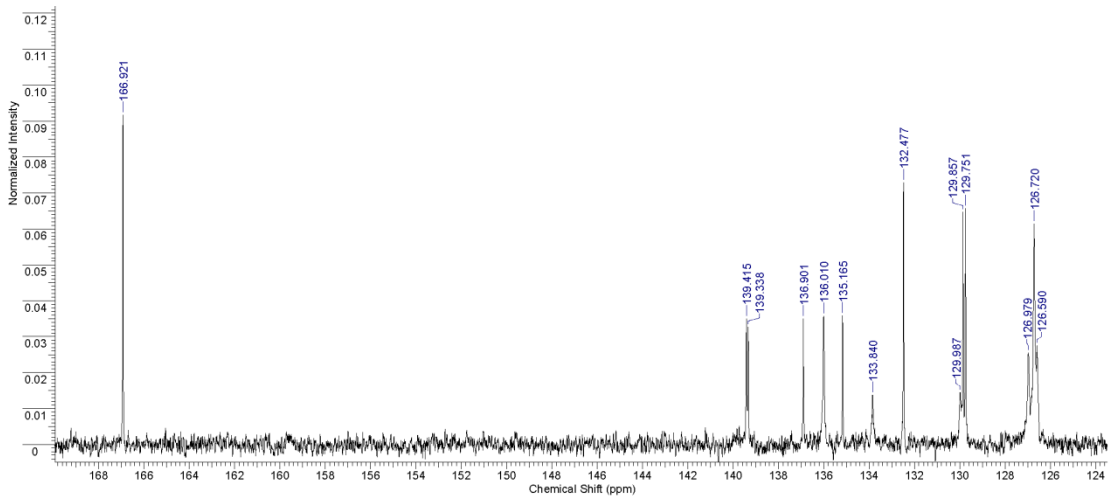

(b)

Figure S2. (a) ^{13}C NMR spectrum of 5,5',5"-(benzene-1,3,5-triyltris(anthracene-10,9-diyl))triisophthalic acid (H_6BTAT) in DMSO-d_6. (b) The ^{13}C NMR spectrum in the region 168–124 ppm.

Section 2. Single Crystal X-ray and PXRD Structures for MFM-132

Single crystal X-ray crystallographic data for MFM-132 were collected at 120 and 298 K on a DECTRIS Pilatus pixel array detector using synchrotron radiation on Beamline I19 (EH1) at Diamond Light Source. Data processing was conducted by using *xia2*,[2] an automated system for macromolecular crystallography. The structures of MFM-132 (at two temperatures) were solved by direct methods and refined by full-matrix least-squares on F^2 using *SHELXTL*-2014[3]. Hydrogen atoms were placed in calculated positions and refined using a riding model with isotropic displacement parameters set to 1.2 × U_{eq} of their carrier atoms. The solvent molecules are highly disordered and could not be modelled as discrete atomic sites. Contributions to scattering due to these solvent molecules were removed using the SQUEEZE routine of PLATON,[4] and the structure was then refined using the solvent-free diffraction intensities. The final formula was calculated from the SQUEEZE results combined with elemental analysis data. Crystal data are summarized in Table S1. The CIF files can be obtained free of charge from the Cambridge Crystallographic Data Centre via www.ccdc.cam.ac.uk/data_request/cif (CCDC 1499823 and 1499824).

At 120 K, MFM-132 crystallizes in cubic space group Fm-3m with a = 46.198(3) Å and is isostructural with MFM-112 (NOTT-112),[5] featuring the same (3,24)-connected network. One C_3-symmetric $BTAT^{6-}$ unit comprising three coplanar isophthalate moieties is connected with 6 $[Cu_2(O_2CR)_4]$ paddlewheels, forming a hexagonal linker face. Surprisingly, unlike the linker face in MFM-112, where the linker is almost flat within the plane defined by the three isophthalates in the linker, the linker in MFM-132 at 120 K forms a more convex shape despite the rigidity of the organic linker (Fig. S3). The $BTAT^{6-}$ unit is contracted towards the centre of the molecule, bringing three peripheral anthracene panels close with each other and forcing the central phenyl ring protruding out the plane formed by the three isophthalate units in the linker unit. The three anthracene units are almost perpendicular with the periphery arms of the linker face and have been compacted to close proximity with H•••H (from two adjacent anthracene rings) distance of 2.6 Å, which is just slightly larger than the sum of the van der Waals radii of two hydrogen atoms (2.4 Å). The force for the contraction and curvature of the linker probably comes from the strong interactions between the anthracene moieties with the guest solvent molecules present in the pore at low temperature (120 K) and the intrinsic flexible nature of the (3,24)-connected network comprising large aromatic substituents.[6] Single crystal X-ray

diffraction data collected at 298 K reveals a distinct unit cell expansion in as-synthesized MFM-132. The framework reveals the same structural feature as at 120 K, but with ~0.7 Å increase in unit cell parameter, *a* = 46.945(5) Å. Unlike the more convex shape of the hexagonal face in the solvent-containing structure at 120 K, the linker face is almost flat with the linker arms being fully stretched in the framework at 298 K. The separation of two adjacent anthracene units in the central core of the linker increases to 2.9 Å (the distance between the closest H atoms from two anthracene units in the same linker), indicating a less steric repulsion between the adjacent anthracene rings.

Activation and Porosity of MFM-132a. The as-synthesised MFM-132 was fully exchanged with acetone and then subjected to thermal evacuation under dynamic vacuum at 100 °C for 24 h to afford the desolvated MFM-132a. The synchrotron PXRD pattern for MFM-132a were analysed by Rietveld refinement based on the single crystal structure model at 298 K. MFM-132a retains high crystallinity and shows the same structural features (space group and atoms connectivity) as the single crystal form. Interestingly, MFM-132a shows slightly enlarged unit cell parameter *a* = 47.1567(5) Å compared to the single crystal structure for the solvated form. After activation, the linker face in MFM-132a is completely flat with the linker arms being fully stretched. The separation of two adjacent anthracene units in the central core of the linker in MFM-132a increases to 3.8 Å compared to the solvated form. The activated phase retains its framework rigidity at various temperatures (298 K and 400 K), as confirmed by the variable-temperature synchrotron PXRD analysis (see below). MFM-132a shows permanent microporosity as revealed by the N_2 adsorption at 77 K which shows typical Type I isotherm, indicative of the characteristics for a microporous material.

Table S1. Single crystal X-ray data and structure refinement details for as-synthesized MFM-132 at 120 K and 298 K.

	MFM-132 (120 K)	**MFM-132 (298 K)**
Chemical formula	$C_{99}H_{105}Cu_3N_9O_{24}$	$C_{99}H_{105}Cu_3N_9O_{24}$
Formula weight	1995.53	1995.53
Temperature	120 (2) K	298(2) K
Radiation type	Synchrotron	Synchrotron
λ (Å)	0.6889	0.6889
Crystal System	Cubic	Cubic
Space Group	*Fm-3m*	*Fm-3m*
Unit Cell Dimensions	$\alpha = \beta = \gamma = 90^o$ $a = b = c = 46.198(3)$ Å	$\alpha = \beta = \gamma = 90^o$ $a = b = c = 46.945(5)$ Å
Volume	98598(22) Å^3	103460(36)
Z	32	32
Density	1.075 g/cm^3	1.025 g/cm^3
Absorption coefficient	0.53 mm^{-1}	0.505 mm^{-1}
F(000)	33312	33312
Crystal Size	0.05 × 0.05 × 0.05 mm^3	0.05 × 0.05 × 0.05 mm^3
Reflections collected	133972	245835
Independent reflections	1686 [R_{int} = 0.222]	1906 [R_{int} = 0.067]
Absorption correction	multi-scan	multi-scan
Refinement method	Full-matrix least-squares on F^2	Full-matrix least-squares on F^2
Data / restraints / parameters	2124 / 131/ 191	3111/223/174
GOF on F^2	1.428	1.099
Final *R* indices [$I > 2\sigma(I)$]	R_1 = 0.128, wR_2 = 0.345	R_1 = 0.085, wR_2 = 0.288
Final *R* indices (all data)	R_1 = 0.145, wR_2 = 0.366	R_1 = 0.102, wR_2 = 0.304
Difference Fourier map: maximum peak, minimum trough (e Å^{-3})	0.561, –0.188	0.422, –0.316
CCDC	1499823	1499824

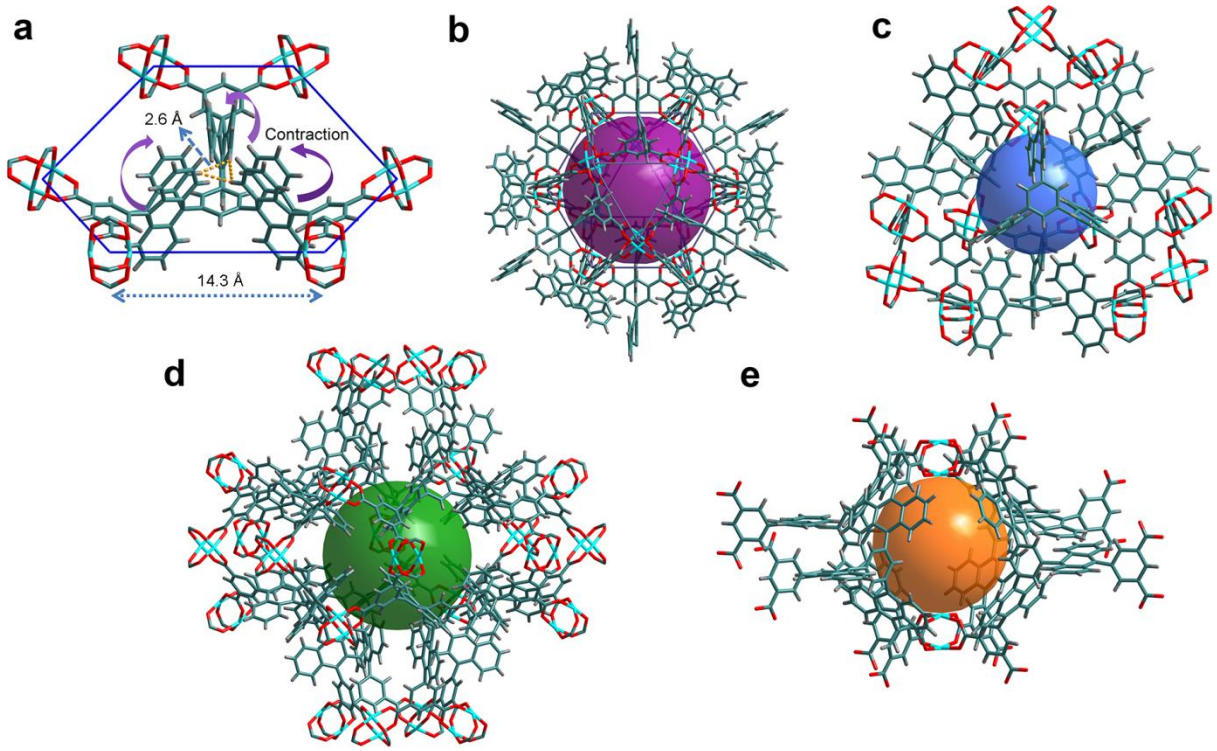

Figure S3. View of the single crystal structure of MFM-132 solved from the X-ray diffraction data collected at 120 K. (a) View of the hexagonal linker face in MFM-132. View of four different types of cages in MFM-132: (b) Cage A; (c) Cage B; (d) Cage C and (e) Cage D. The coordinated H_2O molecules on Cu(II) are removed for clarity.

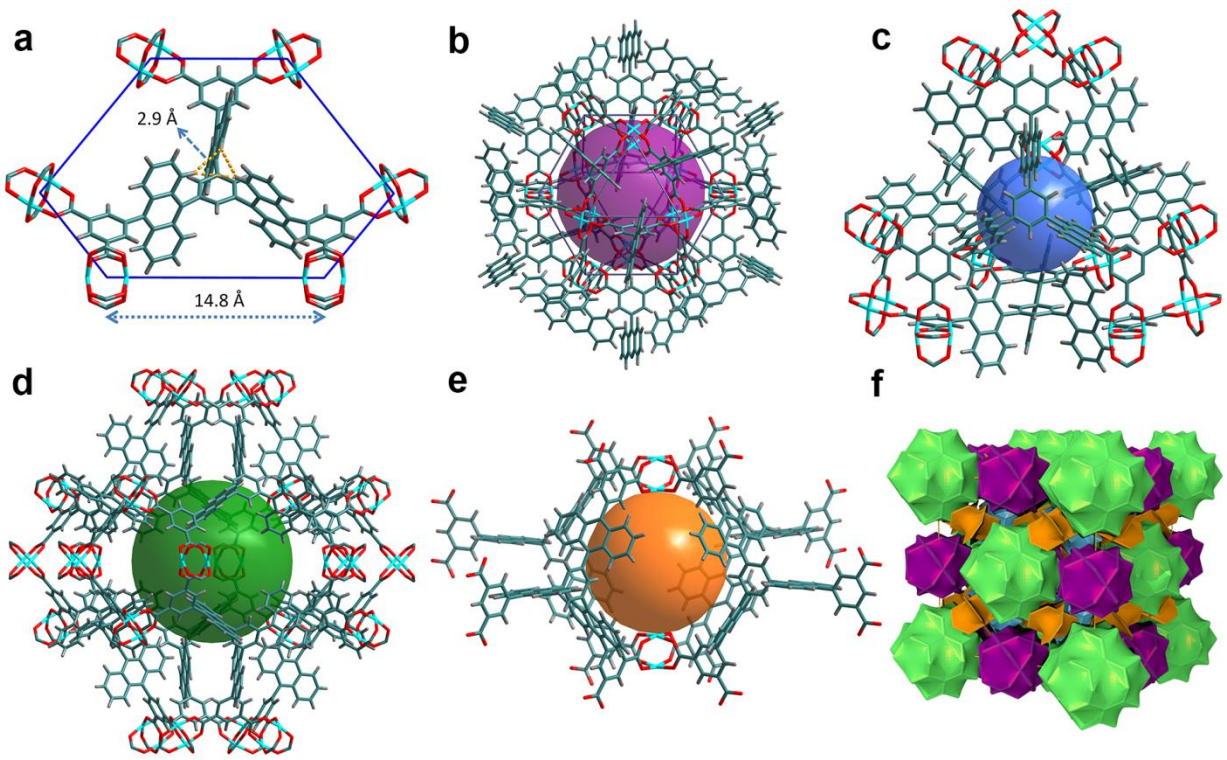

Figure S4. View of the single crystal structure of MFM-132 solved from the X-ray diffraction data collected at 298 K. (a) View of the hexagonal linker face in MFM-132. View of the four different types of cages in MFM-132: (b) Cage A; (c) Cage B; (d) Cage C and (e) Cage D. The coordinated H_2O molecules on Cu(II) are removed for clarity. (f) The natural tilling of the four types of cages in the (3,24)-connected network .

High-Resolution Synchrotron Powder X-ray Diffraction. High-resolution synchrotron powder X-ray diffraction (PXRD) data were collected at Beamline I11 of Diamond Light Source using multi-analysing crystal-detectors (MACs)[7] and monochromatic radiation [λ = 0.826651(5) Å]. The PXRD measurements were carried out in capillary mode and the temperature controlled by an Oxford Cryosystems open-flow nitrogen gas cryostat. In a typical experiment, the powder sample of acetone-exchanged MFM-132 (2–4 mg) was dried in air and ground briefly before loading into a borosilicate capillary tube (0.7 mm in diameter), which was then mounted on a gas cell equipped with a gas control panel.

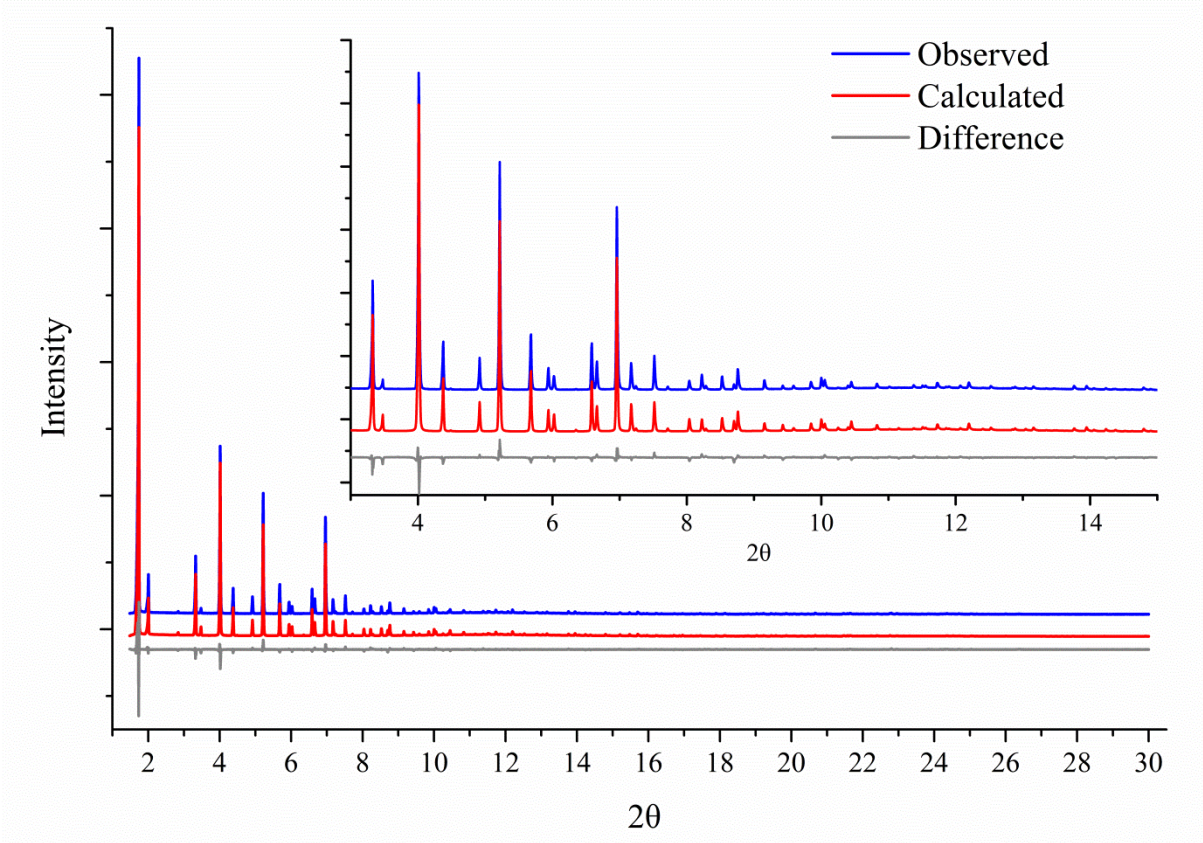

Figure S5. Rietveld refinement of MFM-132a using high-resolution synchrotron PXRD data. The experimental data for MFM-132a were collected at 298 K [radiation wavelength: λ = 0.826651(5) Å]. The *R* values for the final refinement: R_p = 5.89%, R_{wp} = 8.37%, R_{exp} = 2.66%; GoF = 3.15.

Table S2. Crystallographic parameters of MFM-132a from synchrotron X-ray powder data [space group *Fm-3m*, No. 225, a = 47.1567(5) Å, CCDC 1499825].

atom	site	x	y	z	occupancy
Cu1	*48i*	0.3418(8)	0.1582(8)	0	1.0
Cu2	*48i*	0.3833(8)	0.1167(8)	0	1.0
O1	*192l*	0.3242(12)	0.1342(8)	0.0245(11)	1.0
O2	*192l*	0.3629(9)	0.1027(11)	0.0297(12)	1.0
C1	*192l*	0.3378(7)	0.1131(6)	0.0375(8)	1.0
C2	*96k*	0.3352(6)	0.0752(4)	0.0752(4)	1.0
H2A	*96k*	0.3529(17)	0.0656(9)	0.0656(9)	1.0
C3	*192l*	0.3235(5)	0.0998(4)	0.0634(4)	1.0
C4	*192l*	0.2999(5)	0.1126(3)	0.0762(4)	1.0
H4A	*192l*	0.2911(9)	0.1311(16)	0.0674(9)	1.0
C5	*96k*	0.2881(5)	0.1008(3)	0.1008(3)	1.0
C6	*96k*	0.2621(4)	0.1149(3)	0.1149(3)	1.0
C7	*192l*	0.2364(4)	0.1124(3)	0.1002(3)	0.5
C8	*192l*	0.2356(5)	0.0983(3)	0.0741(3)	0.5
H8A	*192l*	0.2542(17)	0.0897(8)	0.0654(8)	0.5
C9	*192l*	0.2098(5)	0.0958(3)	0.0594(3)	0.5
H9A	*192l*	0.2092(6)	0.0853(10)	0.0398(18)	0.5
C10	*192l*	0.1850(4)	0.1073(3)	0.0709(3)	0.5
H10A	*192l*	0.1657(18)	0.1054(4)	0.0599(10)	0.5
C11	*192l*	0.1858(3)	0.1214(2)	0.0971(2)	0.5
H11A	*192l*	0.1672(17)	0.1300(8)	0.1057(8)	0.5
C12	*192l*	0.2115(3)	0.1239(2)	0.1118(2)	0.5
C13	*96k*	0.2124(3)	0.1379(2)	0.1379(2)	1.0
C14	*192l*	0.2381(3)	0.1405(2)	0.1526(2)	0.5
C15	*192l*	0.2630(3)	0.1290(3)	0.1411(3)	0.5
C16	*192l*	0.2887(4)	0.1315(4)	0.1558(4)	0.5
H16A	*192l*	0.3073(17)	0.1229(9)	0.1472(9)	0.5
C17	*192l*	0.2895(4)	0.1456(4)	0.1820(4)	0.5
H17A	*192l*	0.3088(17)	0.1475(5)	0.1930(11)	0.5
C18	*192l*	0.2647(4)	0.1571(3)	0.1935(3)	0.5
H18A	*192l*	0.2653(4)	0.1676(10)	0.2131(18)	0.5
C19	*192l*	0.2389(3)	0.1545(3)	0.1788(3)	0.5
H19A	*192l*	0.2203(17)	0.1631(8)	0.1874(8)	0.5
C20	*96k*	0.18637(17)	0.14996(16)	0.14996(16)	1.0
C21	*96k*	0.17424(16)	0.13783(17)	0.17424(16)	1.0
H21A	*96k*	0.1833(8)	0.1196(16)	0.1833(8)	1.0

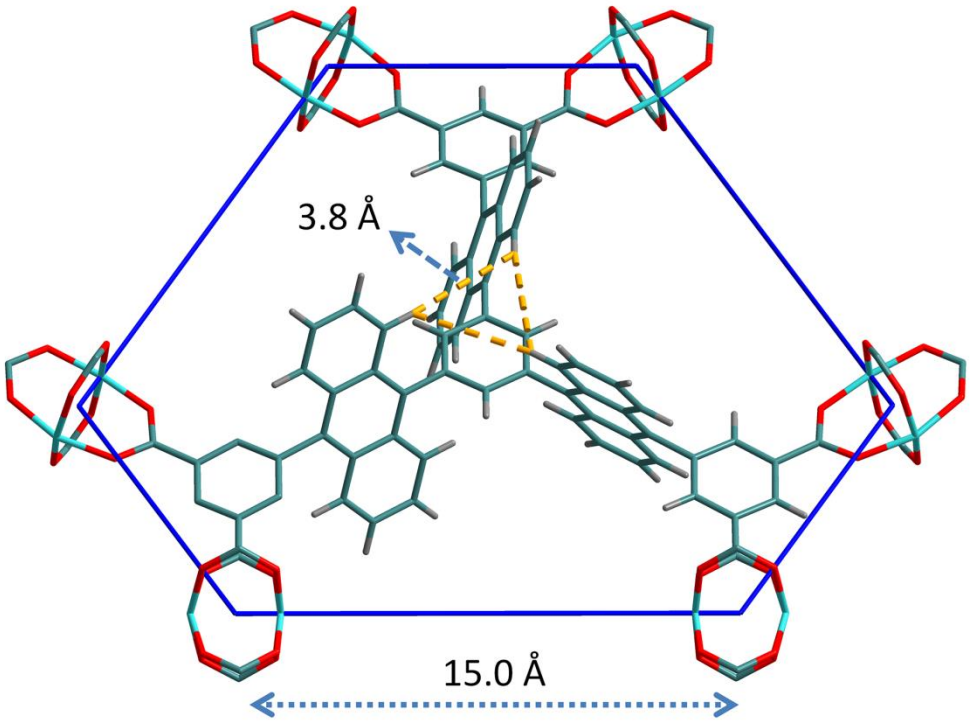

Figure S6. View of the linker structure in the activated form MFM-132a (solved by the synchrotron PXRD data collected at room temperature).

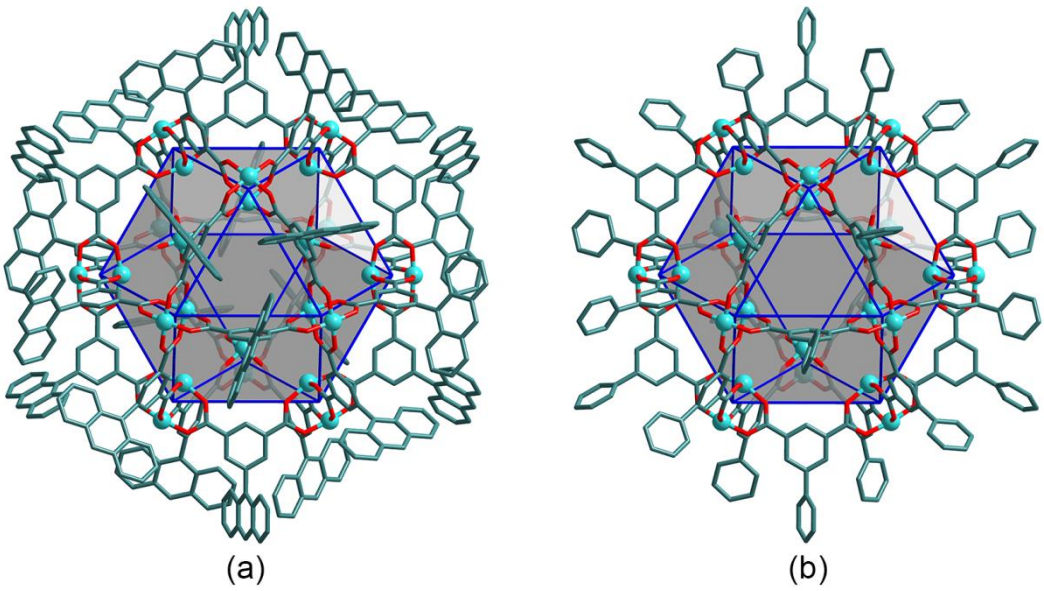

Figure S7. Comparison of the cuboctahedral cage in (a) MFM-132a and (b) MFM-112.

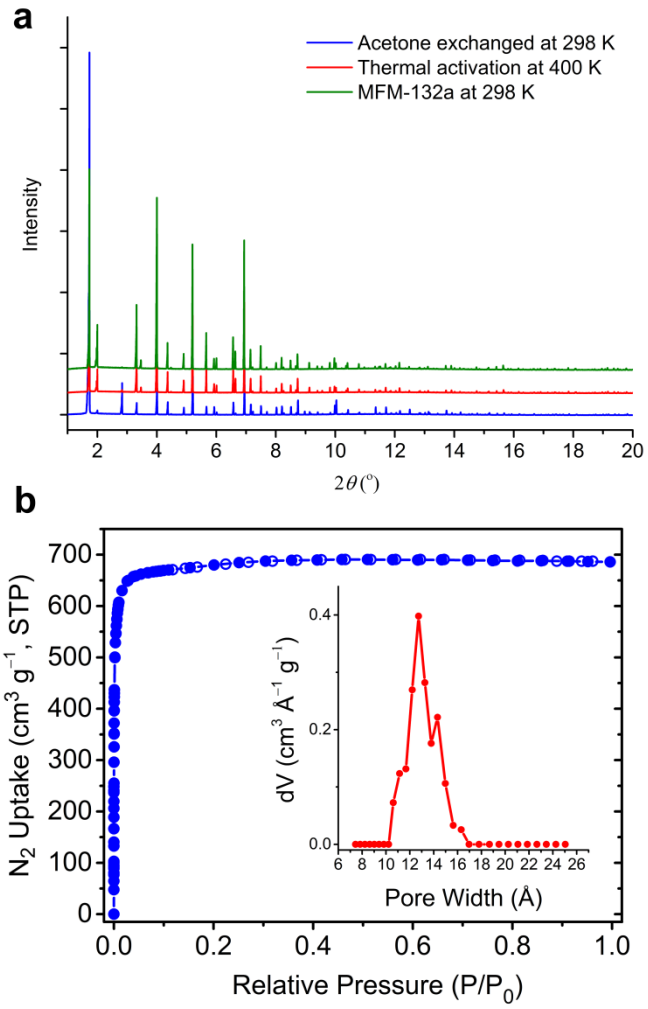

Figure S8. (a) Synchrotron PXRD patterns for acetone-exchanged MFM-132, the sample during thermal activation at 400 K, and activated MFM-132a; (b) N_2 isotherm at 77 K for MFM-132a and pore size distribution (shown in the inert chart).

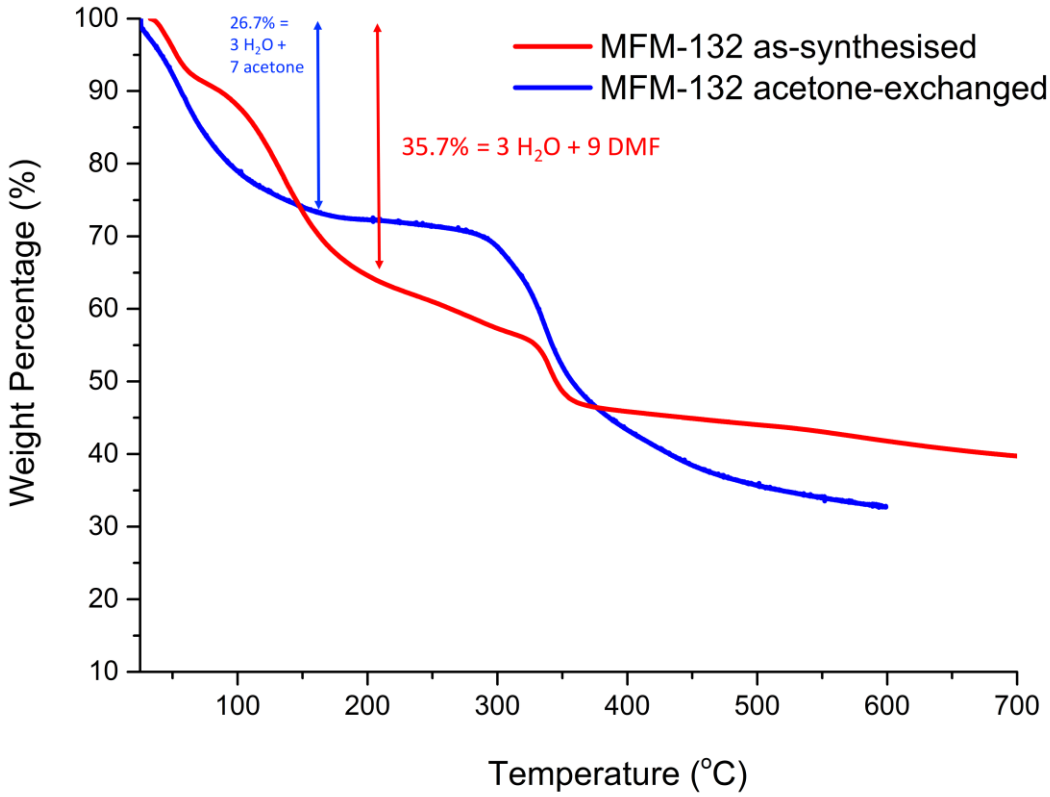

Figure S9. TGA plots for the as-synthesised and acetone-exchanged MFM-132 under N_2 flow at rate of 20 mL min^{-1} with heating rate of 5 °C min^{-1}. The red arrow indicates the loss of 3 H_2O and 9 DMF molecules per formula at 200 °C from the as-synthesized MFM-132; the blue arrow indicates the loss of 3 H_2O and 7 acetone molecules per formula at 170 °C in the acetone-exchanged MFM-132.

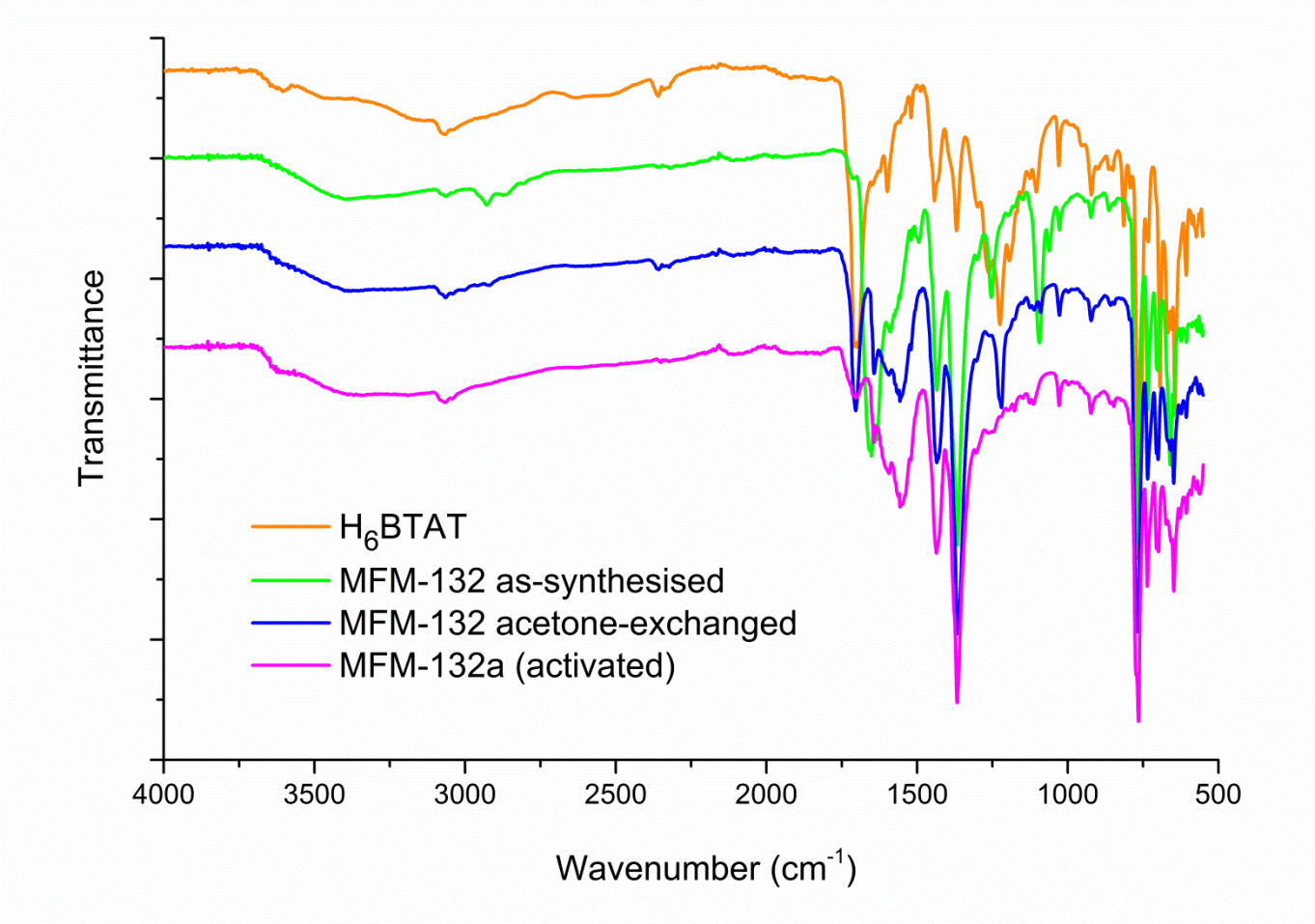

Figure S10. IR spectra for the ligand H_6BTAT, as-synthesised and acetone-exchanged MFM-132 and activated MFM-132a.

Section 3. CH_4 Adsorption

Gravimetric Gas Sorption Measurements. CH_4 isotherms were collected using an IGA gravimetric adsorption apparatus (Hiden) over the pressure range 0–20 bar in a clean ultra-high-vacuum system (10^{-7} mbar) with a diaphragm and turbo pumping system. Approximately 120 mg of solvent-exchanged sample was loaded into the sample basket within the adsorption instrument and then degassed under dynamic vacuum at 100 °C for 24 h to obtain the fully desolvated sample.

The temperature-dependent adsorption data were analyzed using the virial equation:[8]

$$\ln\left(\frac{n}{p}\right) = A_0 + A_1 n + A_2 n^2 + \cdots$$

where p is pressure, n is the amount adsorbed and A_0, A_1, *etc*. are virial coefficients. The enthalpy of adsorption at zero coverage was determined from the relationship:

$$\delta A_0 = R Q_{st}^{n=0} \delta(T^{-1})$$

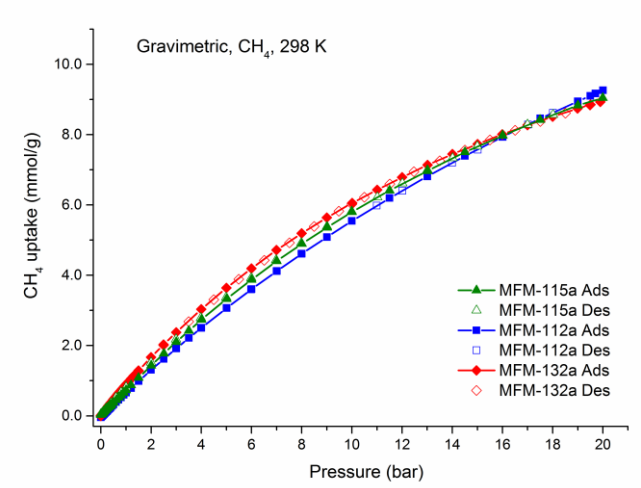

Figure S11. Sorption isotherms (total uptake) for CH_4 in MFM-112a, MFM-115a and MFM-132a at 298 K using the IGA system (Ads = Adsorption; Des = Desorption).

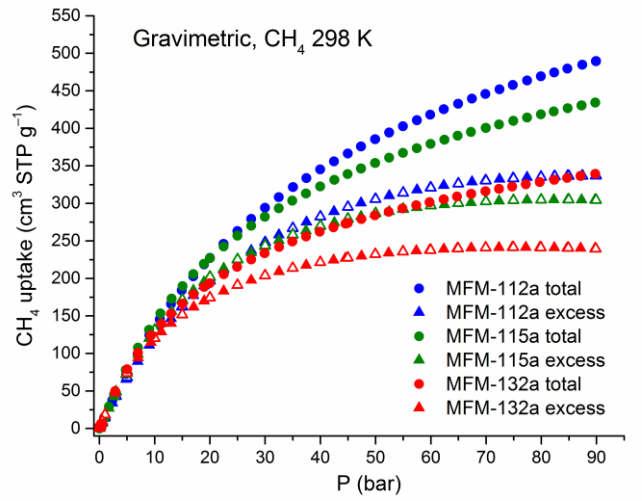

Figure S12. High-pressure sorption isotherms for CH_4 in MFM-112a, MFM-115a and MFM-132a at 298 K using a XEMIS gravimetric sorption analyzer (Hiden Isochema). The total uptake is given by $n_T = n_E + \rho_{CH4}V$ in which n_E is the excess uptake measured from the experiments, ρ_{CH4} is the bulk density of CH_4, and V is the pore volume obtained from the N_2 isotherms. Density of CH_4 at 0–90 bar and 298 K was obtained from the National Institute of Standards and Technology (NIST) of the USA from website: http://webbook.nist.gov/chemistry/fluid/.

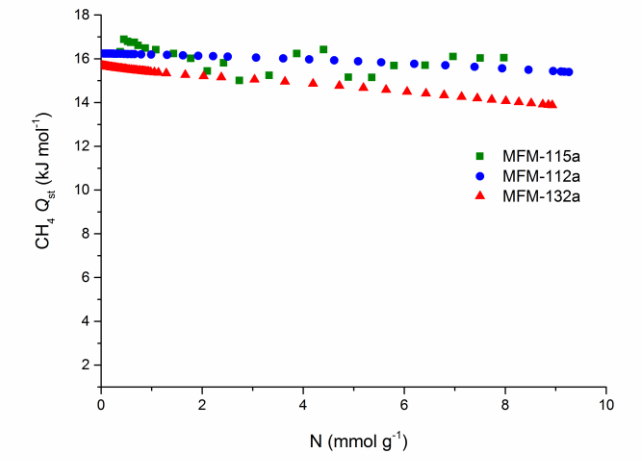

Figure S13. Isosteric heat of adsorption of CH_4 in MFM-112a, MFM-115a and MFM-132a.

Section 4. Synthesis of Partially Deuterated MFMs Series

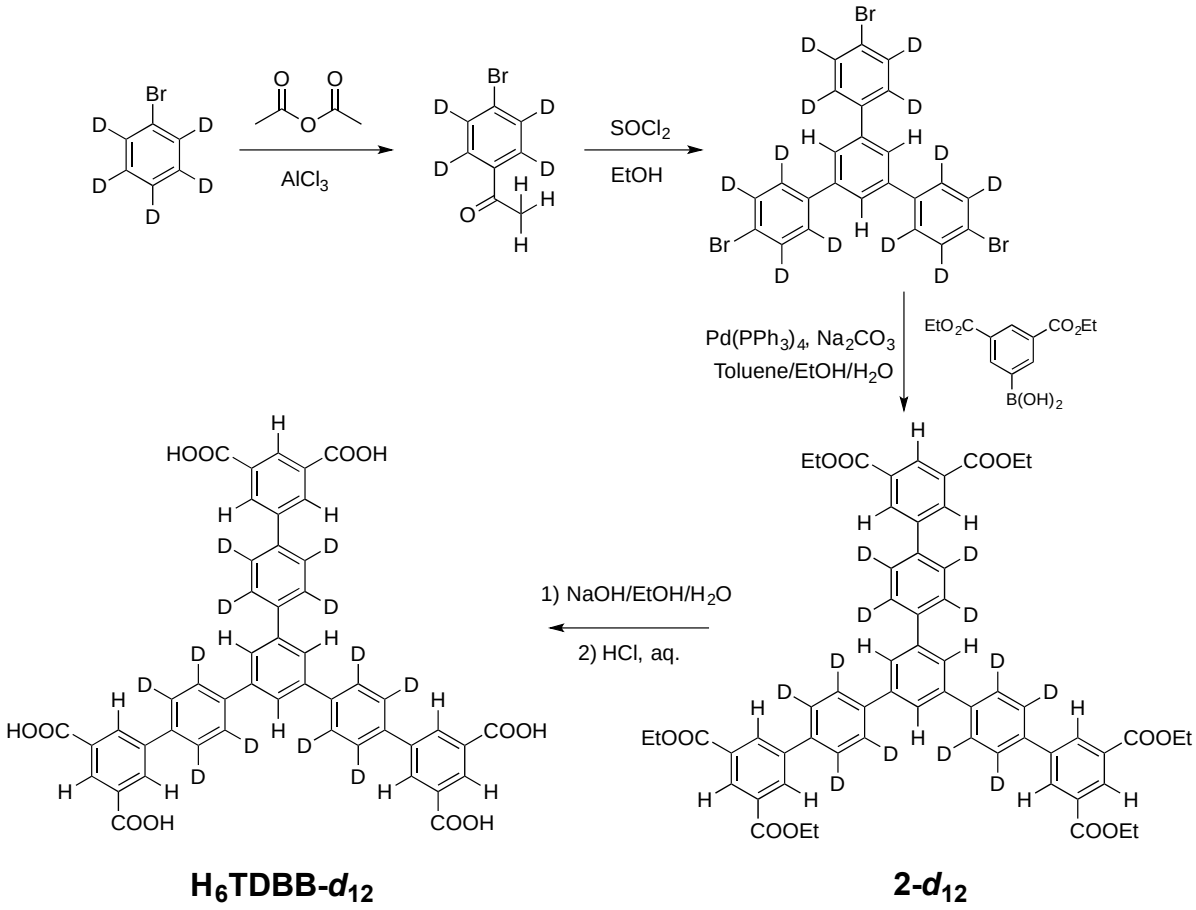

Scheme S2. Synthesis of the hexacarboxylate linker H_6TDBB-d_{12}.

Synthesis of 2-d_{12}. Tris(4-bromophenyl)benzene-d_{12} was synthesised by using the same method for the non-deuterated tris(4-bromophenyl)benzene.[9] Tris(4-bromophenyl)benzene-d_{13} (1.5 g, 2.7 mmol), diethylisophthalate-5-boronic acid (2.8 g, 10.5 mmol) and Na_2CO_3 (2 M, 50 mL) were mixed in toluene/EtOH (1 : 1, 150 mL), and the mixture de-aerated by bubbling Ar through it for 10 mins. [$Pd(PPh_3)_4$] (0.15 g, 0.13 mmol) was added to the reaction mixture, and the mixture heated at 90 °C for 48 h under Ar, after which 1,4-dioxane was removed under vacuum. The reaction mixture was treated with a mixture of CH_2Cl_2/H_2O (100/100 mL) and extracted twice with CH_2Cl_2 (2 × 30 mL). The combined organic extracts were washed with brine and dried over $MgSO_4$. After filtration, the solvent was removed by evaporation and the residue purified by column chromatography over silica gel using hexane/ethyl acetate (3:1) as eluent to

afford the pure product (2.2 g, 82% yield) as a white solid. ^{13}C NMR (75 MHz, $CDCl_3$, ppm): δ 165.84, 141.82, 141.20, 140.64, 138.36, 132.09, 131.61, 129.39, 127.64, 127.29, 125.25, 61.52, 14.39.

Synthesis of 1,3,5-tris(3′,5′-dicarboxy[1,1′-biphenyl]-4-yl)benzene-d_{12} (H_6TDBB-d_{12}). Compound 2-d_{12} (1.5 g, 1.6 mmol) was suspended in a mixture of THF (50 mL) and EtOH (50 mL), to which was added an aqueous solution of NaOH (2 M, 50 mL). The mixture was stirred under reflux overnight and the volatiles were removed under vacuum. Concentrated HCl solution was added to the remaining aqueous solution until the solution was at pH = 3. The precipitate was collected by filtration, washed with water and EtOH, and dried to give the product as a white solid (1.2 g, 98%). ^{1}H NMR (300 MHz. DMSO-d_6, ppm): δ 8.45 (t, J = 1.5 Hz, 3 H), 8.42 (d, J = 1.5 Hz, 6 H), 8.01 (s, 3 H); ^{13}C NMR (75 MHz, DMSO-d_6, ppm): δ 167.04, 141.40, 140.92, 140.06, 137.89, 132.57, 131.56, 129.33, 128.04, 127.44, 124.87.

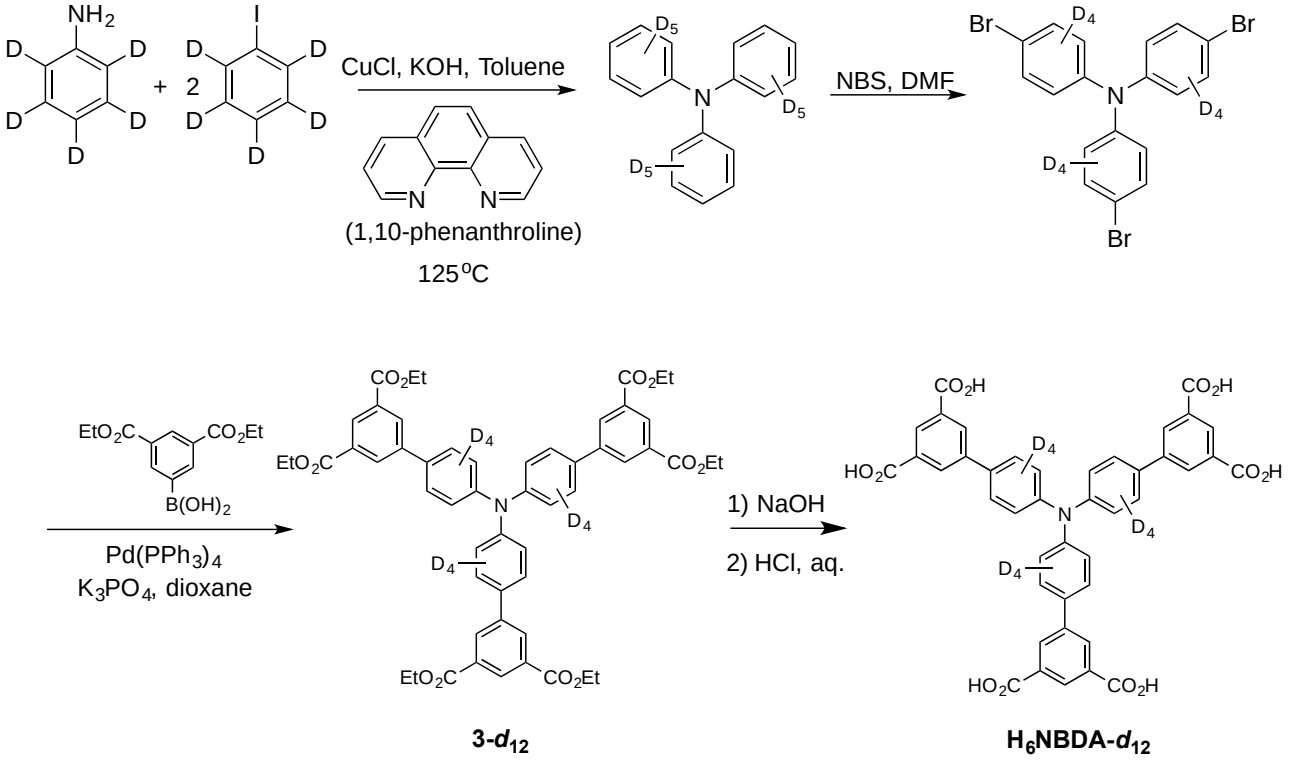

Scheme S3. Synthesis of the partially deuterated linker H_6NBDA-d_{12}.

Synthesis of 3-d_{12}. Tris(phenyl-d_5)amine was synthesized by ligand-accelerated catalysis of the Ullmann condensation reported by Goodbrand and Hu.[10] A mixture of tris(4-bromophenyl-2,3,5,6-d_4)amine (0.5 g, 1.0 mmol), diethylisophthalate-5-boronic acid (0.97 g, 3.6 mmol), [$Pd(PPh_3)_4$] (0.07 g, 0.06 mmol), K_3PO_4 (1.6 g, 7.5 mmol), *p*-dioxane (40 mL), and H_2O (20 mL) was heated at reflux under Ar for 18 h before H_2O (100 mL) was added. The reaction mixture was extracted twice with CH_2Cl_2, and the combined organic extracts were washed with brine and dried over $MgSO_4$. After filtration, the solvent was removed by evaporation and the residue purified by column chromatography over silica gel using hexane/CH_2Cl_2 (1:1) as eluent to afford the pure product (0.7 g, 75%) as a light yellow solid. ^{1}H NMR (300 MHz, $CDCl_3$, ppm): δ 8.65 (t, J = 1.5 Hz, 3 H), 8.48 (d, J = 1.5 Hz, 6 H), 4.47 (q, J = 6.9 Hz, 12 H), 1.46 (t, J = 6.9 Hz, 18 H); ^{13}C NMR (75 MHz, $CDCl_3$, ppm): δ 165.89, 147.17, 141.10, 133.77, 131.73, 131.51, 128.92, 127.68, 124.17, 61.46, 14.38.

Synthesis of 4',4''',4'''''-nitrilotris(([1,1'-biphenyl]-3,5-dicarboxylic acid))-d_{12} (H_6NBDC-d_{12}). A mixture of **3-d_{12}** (0.7 g, 0.76 mmol), aqueous NaOH (0.5 M, 30 mL), and EtOH (30 mL) was heated at 80 °C for 24 h. The EtOH was removed by evaporation and concentrated HCl added to the aqueous residue to pH = 1. The precipitate thus formed was collected by filtration, washed with H_2O, and dried in air to afford the pure product (0.56 g, 98%) as a light yellow solid. ^{1}H NMR (300 MHz, DMSO-d_6, ppm): δ 8.43 (t, J = 1.5 Hz, 3 H), 8.38 (d, J = 1.5 Hz, 6 H); ^{13}C NMR (75 MHz, DMSO-d_6, ppm): δ 167.03, 147.20, 140.80, 133.34, 132.60, 131.22, 128.88, 128.25, 124.50.

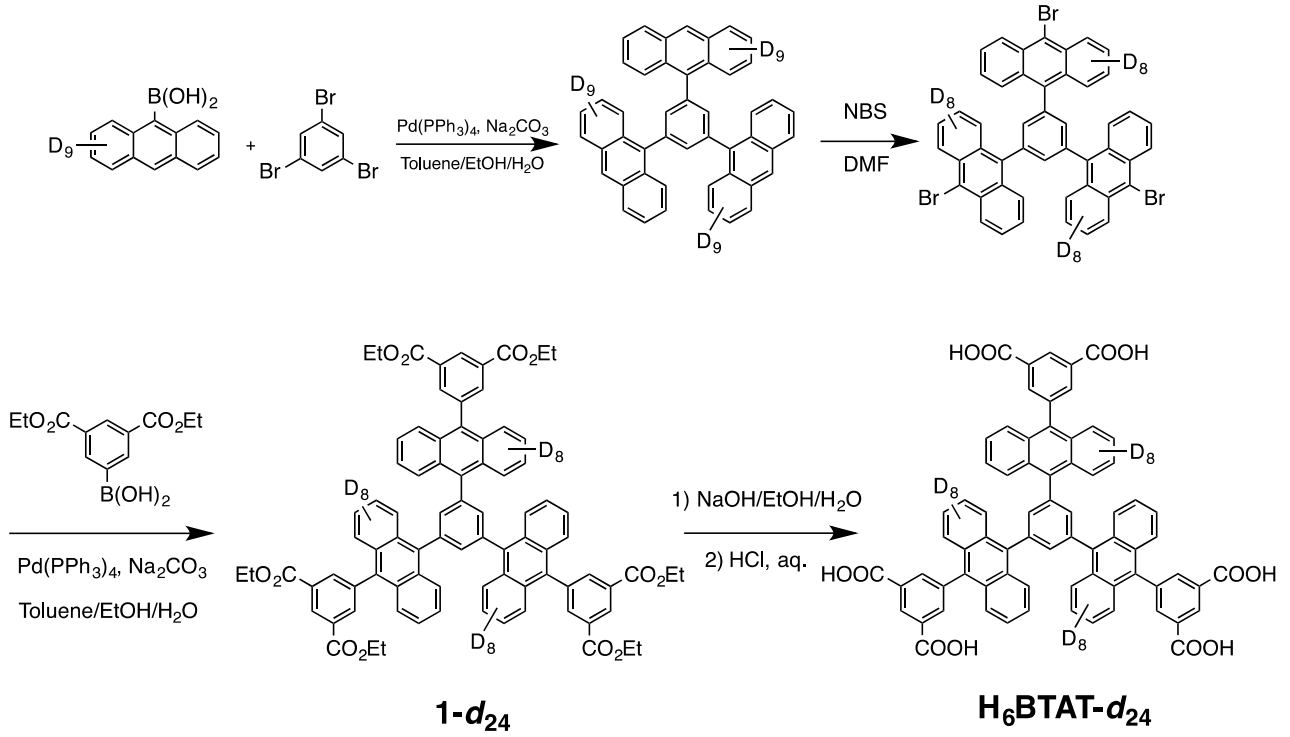

Scheme S4. Synthesis of the partially deuterated linker H_6BTAT-d_{24}.

Synthesis of 1-d_{24}. 1,3,5-tris(10-bromoanthracen-9-yl-1,2,3,4,5,6,7,8-d_8)benzene (TBB-d_{24}) was prepared by using the method reported previously[1] for the non-deuterated 1,3,5-tris(10-bromoanthracen-9-yl)benzene. Here, the synthesis of partially deuterated ester 1-d_{24} is described. A mixture of toluene/EtOH/H_2O (1:1:1 v/v, 50 mL) was purged with Ar for 30 min and transferred subsequently through a cannula to a round-bottomed flask charged with TBB-d_{24} (0.6 g, 0.7 mmol), diethylisophthalate-5-boronic acid (0.66 g, 2.5 mmol), Na_2CO_3 (0.55 g, 5.2 mmol), and [$Pd(PPh_3)_4$] (0.05 g, 0.04 mmol). The resulting mixture was heated under reflux overnight before being cooled to RT and extracted with CH_2Cl_2 (50 mL) and H_2O (50 mL). The aqueous phase was washed twice with CH_2Cl_2 (50 mL). The combined organic phases were washed with H_2O, dried ($MgSO_4$), filtered, and concentrated. The crude product was absorbed on silica-gel and subjected to column chromatography (SiO_2, hexanes/EtOAc = 2:1) to afford compound 1-d_{24} as a light yellow solid (0.8 g, 90 %). ^{1}H NMR (300 MHz, $CDCl_3$, ppm): δ 8.83 (t, J = 1.6 Hz, 3 H), 8.27 (d, J = 1.6 Hz, 6 H), 7.85 (s, 3 H), 4.34 (q, 12 H), 1.31 (t, 18 H).

Synthesis of H_6BTAT-d_{24}. A mixture of 1-d_{24} (0.8 g, 0.62 mmol), aqueous NaOH (0.5 M, 30 mL), and EtOH (30 mL) was heated at 85 °C for 24 h. The EtOH was removed by evaporation and concentrated HCl added to the aqueous residue to pH = 1. The precipitate thus formed was collected by filtration, washed with H_2O, and dried in air to afford the pure product (0.69 g, 99%) as a light yellow solid. ^{1}H NMR (300 MHz, DMSO-d_6, ppm): δ 13.48 (s, 6 H), 8.72 (t, J = 1.6 Hz, 3 H), 8.19 (d, J = 1.6 Hz, 6 H), 7.84 (s, 3 H); ^{13}C NMR (75 MHz, DMSO-d_6, ppm): δ 166.93, 139.45, 139.36, 136.85, 136.02, 135.09, 133.83, 132.48, 129.98, 129.79, 129.68, 126.24 (low intensity, peaks not resolved).

Preparation of partially deuterated MFMs series: Materials (typically 0.2 g) were obtained in microcrystalline form and good phase purity *via* the experimental procedure described below. The as-synthesised samples were solvent-exchanged by immersing solids in acetone, the process being repeated 6 times over 2 days, and the resulting samples stored under acetone. For all the solid-state ^{2}H NMR experiments, the acetone-exchanged materials were desolvated at 100 °C under dynamic vacuum for 24 h to afford the crystalline materials MFM-112-d_{12}, MFM-115-d_{12} and MFM-132-d_{24}. The PXRD data for the partially deuterated MFM series all match the PXRD patterns simulated from the single crystal structure of the non-deuterated materials. This confirms that the structures of the partially deuterated frameworks are identical to their non-deuterated versions.

Preparation of $[Cu_3(C_{48}H_{12}D_{12}O_{12})(H_2O)_3]$.xDMF (MFM-112-$d_{12}$): H_6TDBB-d_{12} (0.1 g, 0.12 mmol) and $Cu(NO_3)_2$.$3H_2O$ (0.29 g, 1.2 mmol) were mixed and dispersed in *N*,*N*-dimethylformamide (DMF) (50 mL), and HCl (2 M, 0.3 mL) was added to the mixture which was mixed thoroughly. The solution was heated without stirring on an oil bath at 85 °C for 18 h, and a large amount of microcrystalline product precipitated. The blue crystalline product was separated by filtration and washed with warm DMF, and dried briefly in air (75% yield based on the ligand).

Preparation of $[Cu_3(C_{42}H_9D_{12}NO_{12})(H_2O)_3]$.xDMF (MFM-115-$d_{12}$): To a solution of H_6NBDA-d_{12} (0.1 g, 0.13 mmol) and $Cu(NO_3)_2$.$3H_2O$ (0.31 g, 1.3 mmol) in DMF (30 mL) was added HCl (1 M, 0.5 mL). The

mixture was prepared in a pressure flask and heated at 90 °C for 12 h to give pure blue-green crystals (86% yield based on the ligand).

Preparation of $[Cu_3(C_{72}H_{12}D_{24}O_{12})(H_2O)_3]$.xDMF (MFM-132-$d_{24}$): To a solution of H_6NBDA-d_{12} (0.1 g, 0.09 mmol) and $Cu(NO_3)_2$.$3H_2O$ (0.22 g, 0.9 mmol) in DMF (50 mL) was added HCl (2 M, 0.3 mL). The mixture was prepared in a pressure flask and heated at 90 °C for 15 h to give pure blue-green crystals (72% yield based on the ligand).

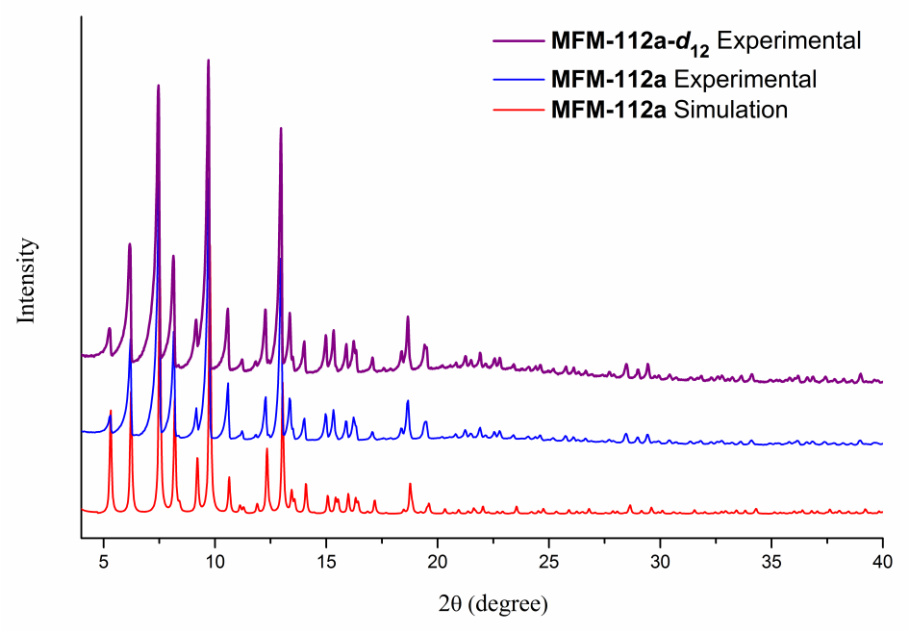

Figure S14. Comparison of the PXRD patterns for MFM-112a-d_{12} and MFM-112a. The experimental PXRD patterns were collected at 298 K.

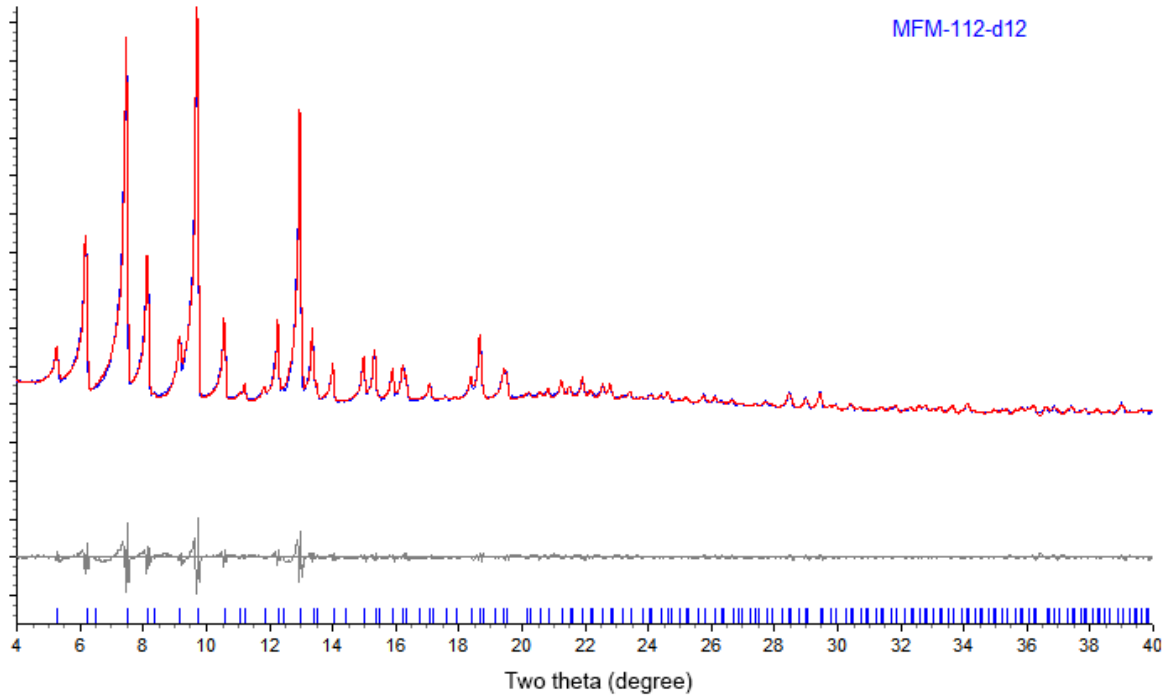

Figure S15. Le Bail refinement of the PXRD pattern for MFM-112-d_{12}. [Space group: *F*m-3m; a = 47.210(7) Å; R_{wp} = 1.54%, R_{exp} = 0.31%; red: experimental; blue: calculated; grey, difference]

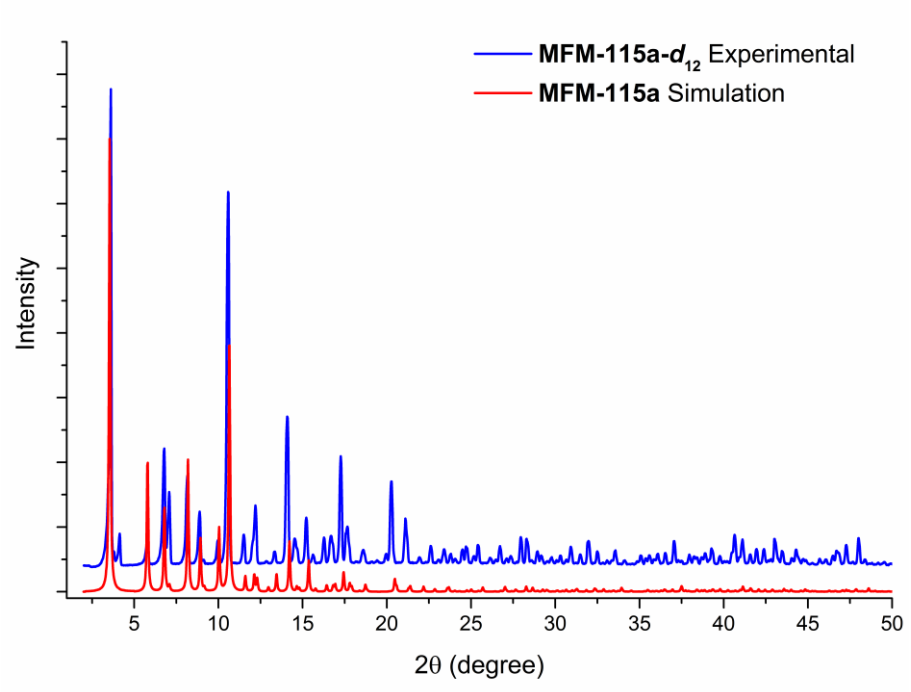

Figure S16. Comparison of experimental PXRD pattern for MFM-115a-d_{12} with the simulation from the single crystal X-ray structure of MFM-115a.

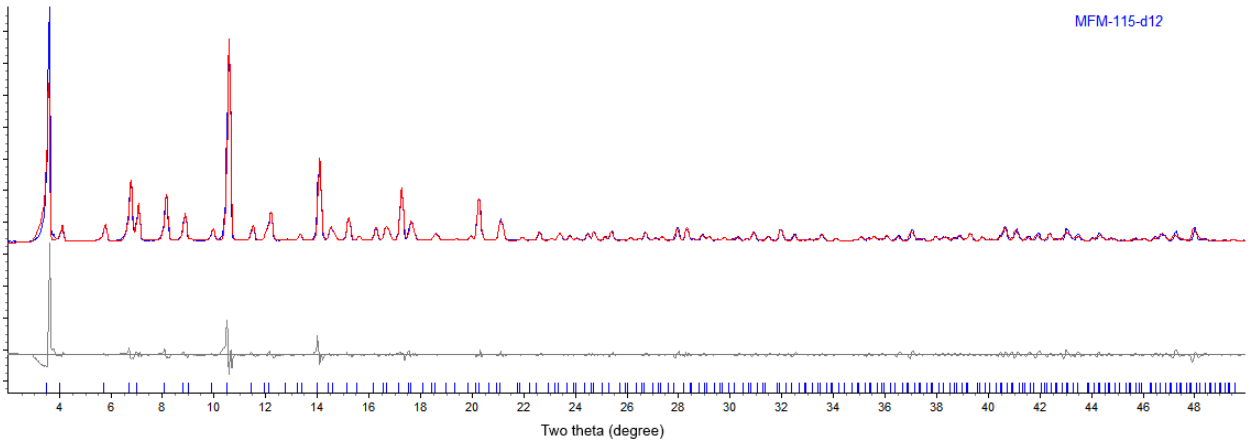

Figure S17. Le Bail refinement of the PXRD pattern for MFM-115-d_{12}. [Space group: *F*m-3m; a = 43.805(5) Å; R_{wp} = 10.12%, R_{exp} = 1.15%; red: experimental; blue: calculated; grey, difference]

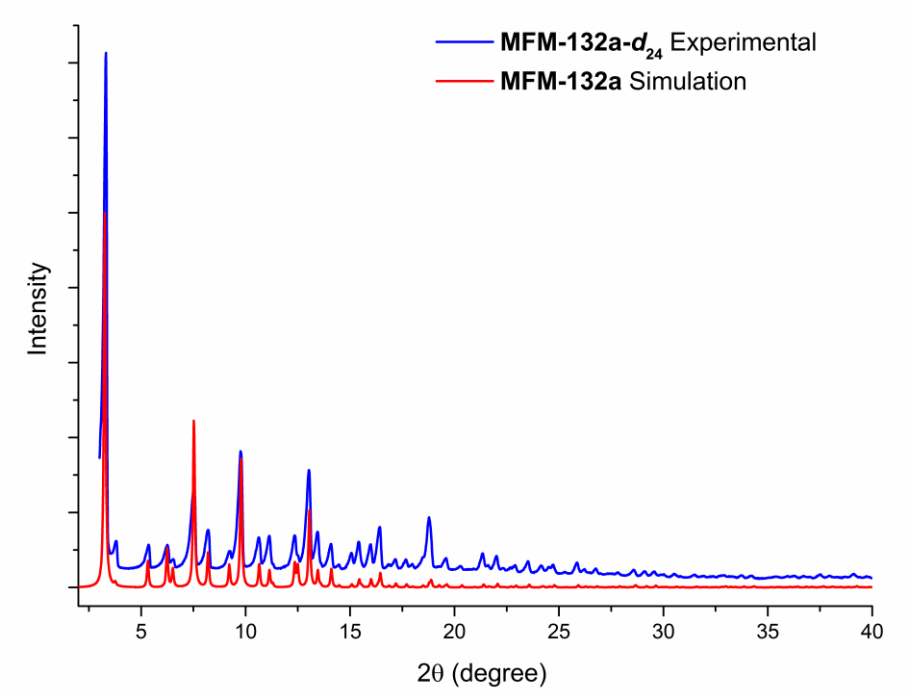

Figure S18. Comparison of experimental PXRD pattern for MFM-132a-d_{24} with the simulation from the single crystal X-ray structure at 298 K.

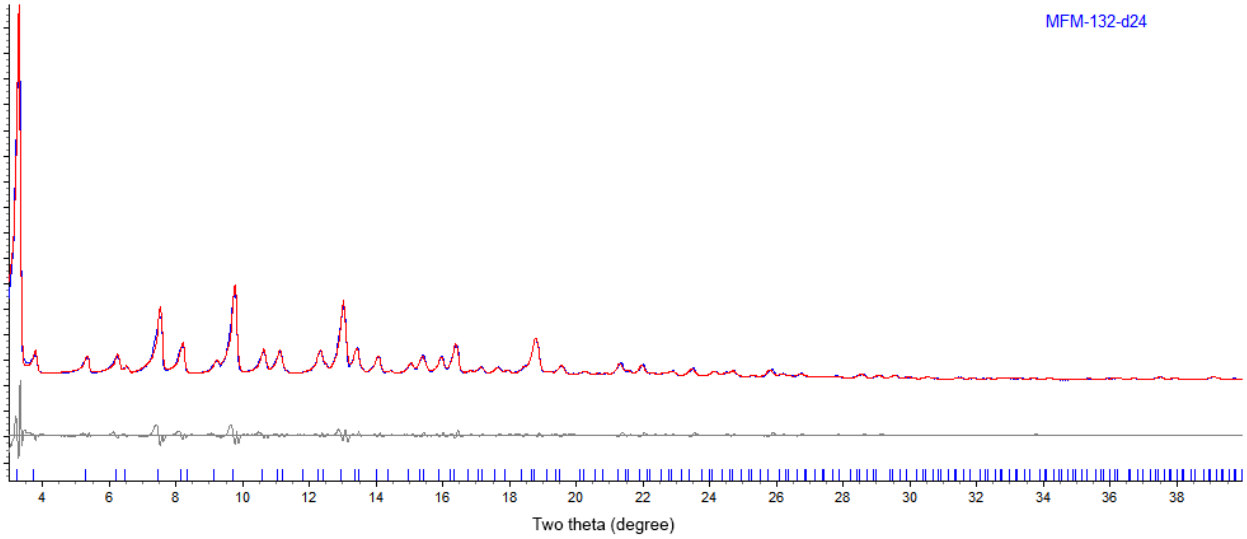

Figure S19. Le Bail refinement of the PXRD pattern for MFM-132-d_{24}. [Space group: *F*m-3m; a = 47.302(8) Å; R_{wp} = 6.49%, R_{exp} = 1.13%; red: experimental; blue: calculated; grey, difference]

Section S5. Solid-State ^{2}H NMR Studies

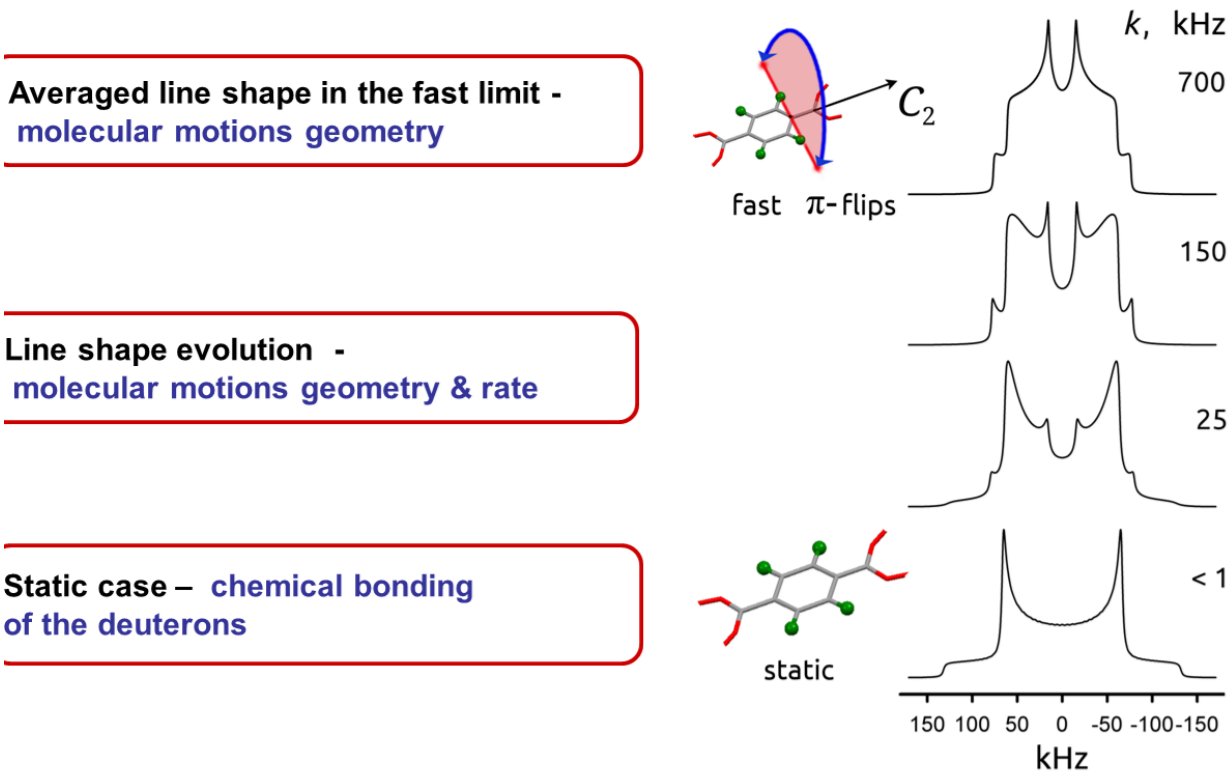

Figure S20. Spectral line shapes measured by ^{2}H NMR spectroscopy depending on the motions rates; an illustrative example for a 2-site 180^o flip of a phenyl ring is given. The line shape develops from a pattern characterized by a nuclear quadrupolar coupling constant Q_0 = 176 KHz and an asymmetry parameter η_0 = 0, typical for a static phenyl ring, up to a strongly narrowed line shape expected for an axial rotation of the phenyl group about a C_2 symmetry axis (Q_1 ~20 kHz~Q_0/8).[11] The narrowed patterns are characterized by a large asymmetry parameter η~0.8, while η~0 is expected for a simple uniaxial (symmetric) jump-rotation model. This indicates that the orientation angles positions are not distributed evenly over the full 360°.

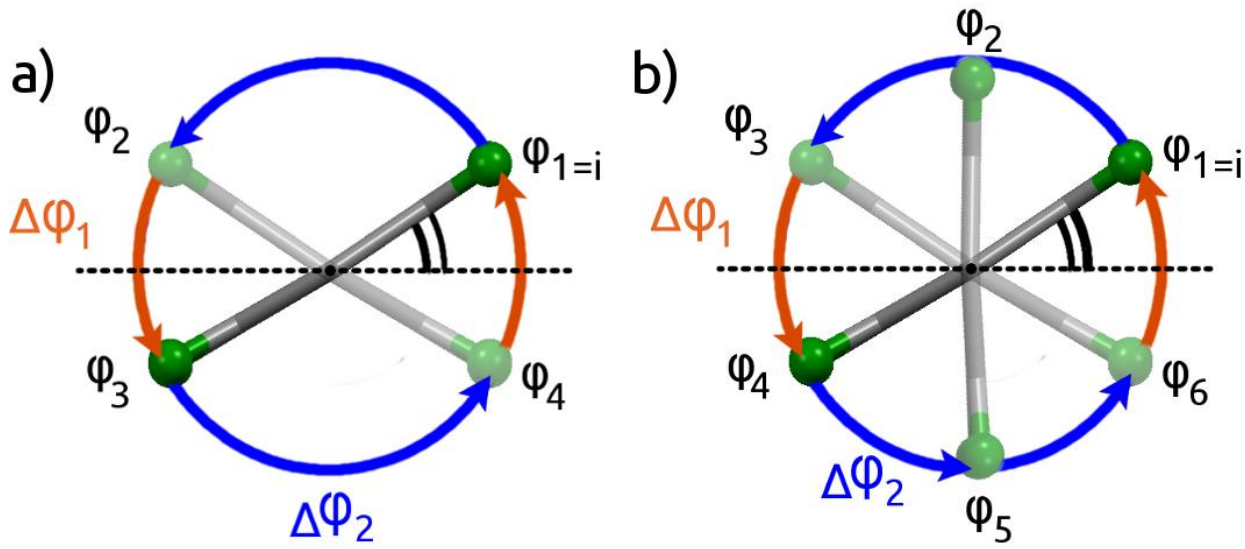

Figure S21. The scheme of stable phenyl ring orientation sites depending on the jump rotation model: the axial jump-rotation about the phenyls symmetry axis C_2 is realized then either by a (a) 4-site exchange motion, or by a (b) 6-site exchange. The distribution of the orientation sites is governed only by the value of the first position $\varphi_1 = \varphi_i$. In each case the motional process is assumed to be governed only by 1 rate constant.

^{2}H NMR spectra line shape simulation:

To understand the detailed mechanism of rotations and their kinetic parameters (the activations barriers and rate constants), a detailed fitting analysis of the ^{2}H NMR spectral line shape across a temperature range was performed. Our FORTRAN simulation routines are based on the general formalism proposed by Abragam[12] and developed in details by Spiess[13] and others.[14–17] The fitted spectra were obtained by Fourier transform of the powder-average over the polar angles θ and φ of the correlation function $G(t,\theta,\varphi)$, which govern the time evolution of the transverse ^{2}H spin magnetization after the solid echo pulse sequence. The correlation function can be computed using the following equation:

$$G(t,q,f) = \sum_{i,j,k}^{1..N} \mathbf{I}_i [\exp(\mathbf{A}t)]_{ij} [\exp(\mathbf{A}t)]_{ij} [\exp(\mathbf{A}^* t)]_{jk} \mathbf{P}_k, \quad (1)$$

where A is a complex matrix composed as follows:

$$\mathbf{A} = \Omega + \mathrm{K}, \quad (2)$$

The diagonal matrix Ω is composed of elements ω_i describing the frequencies of the exchanging sites, and K corresponds to a kinetic matrix that defines the jump rates.

$$\begin{cases} \mathrm{W}_{ii} = i\omega_i - 1/T_2^0 \\ \mathrm{W}_{ij} = 0 \end{cases} \quad \text{and} \quad \begin{cases} \mathrm{K}_{ii} = -\sum_{j \neq i} k_{ij} \\ \mathrm{K}_{ij} = k_{ij} \end{cases}, \tag{3}$$

The $1/T_2^0$ term stands for the residual line width, which reflects the contributions from homo- and hetero-nuclear dipolar interactions of the spin Hamiltonian. **l** is a vector (1,1,…,1) with *N* elements, where *N* is the number of exchange sites. **P** is a vector of equilibrium population of each site $p_{\mathrm{eq}}(i)$. k_{ij} is the exchange rate between sites *i* and *j*. The ^{2}H NMR frequency at the *i*-th site $\omega_i(\theta,\varphi)$ is defined as:

$$\begin{aligned} \omega_i(\theta,\varphi) &= \sqrt{\frac{3}{2}}\frac{1}{2}\sum_{a,b=-2}^{2} q_{2a} D_{ba}(\Omega^i) D_{a0}(\varphi,\theta,0) \\ q_2 &= \left(-\frac{\eta}{2}, 0, \sqrt{\frac{3}{2}}, 0, -\frac{\eta}{2}\right) Q_0 \end{aligned} \tag{4}$$

Here $D_{ba}(\mathrm{W})$ are the Wigner rotation matrices defining the C–D bond orientation for each site and q_2 is static quadrupolar coupling tensor (the Wigner matrices are defined here in a way similar with Spiess's method). If the motion is complex, then the Winger matrix responsible for the transformation of the C–D bond orientation from the principle axis system (PAS, n = 1), frame fixed to a given deuteron (the frame with its Z axis aligned with the C–D bond orientation in our particular case) to the frame attached to the molecular axis system (or the unit cell axis system, n = N), is merely a consequent result of action of multiple Wigner matrices each responsible for a certain rotation, i.e.:

$$D_{ba}(\mathrm{W}) = \sum_{c,d=-2}^{2} D_{bc}(\mathrm{W}^1) D_{cd}(\mathrm{W}^{n\cdots}) D_{da}(\mathrm{W}^N) \tag{5}$$

In other words, to apply such a jump-model concept to the particular case of the dynamics of the phenyl ring, a certain mechanism for these rotations has to be specified: a set of rotational matrices and the rate matrix

that defines the exchange mechanism. Below is a typical and illustrative example of a 180° 2-site exchange jump rotations:

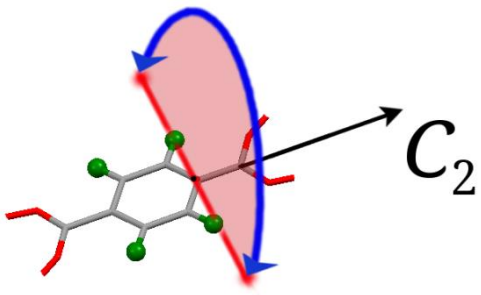

Figure S22. A phenyl ring exhibiting a large-amplitude 180° flips around the C_2 symmetry axis.

The 180° flips around the C_2 axis can be described by a 2 x 2 rate exchange matrix K:

$$K = \begin{bmatrix} -k_1 & k_1 \\ k_1 & -k_1 \end{bmatrix} \qquad (6)$$

In the case when one of the motional processes is characterized by a broad distribution of correlation times the simulation procedure must be modified to take this into account. Physical reasons of such distribution are associated with samples inhomogeneity, either present due to the defects of the crystal structure, or induced by guests or other physical stimuli.

So, the flipping rate $k_f = k_1$ is characterized by such distribution with a distribution width σ. Since the distribution is broad and almost static over the broad temperature region, it can be assumed that the physical reason behind this is the variation in the torsional potential from one site to another. These variations are assumed to be randomly distributed and stable within the material sample. Such assumptions bring us to the log-normal distribution for the flipping rates constant k_f:

$$P(\ln k_f) = \frac{\exp[-\ln^2 k_f / k_{fm}]}{(2p)^{1/2} s_E} \qquad (7)$$

Then to the sum the weighted spectra we write:

$$G(t) = \int_{-\infty}^{\infty} g(t, k_f) P(\ln k_f) d \ln k_f \qquad (8)$$

where $g(t, k_f)$ is the individual simulated FID.

Passing to a discrete distribution we get:

$$G(t) = \sum_{i=1..N} g(t, k_f^i) W^i \qquad (9)$$

Where the individual weights are computed as:

$$W^i = \frac{\int_{\ln k_f^i}^{\ln k_f^{i+1}} P(\ln k) d \ln k}{Norm} \qquad (10)$$

The Norm is calculated as:

$$Norm = \sum_{i=1..N} W^i \qquad (11)$$

Such modification to the original fitting routine allows us to take into account the rate exchange distribution for any motion(s). Within such approach any rate constant will be characterized by 2 parameters: σ —the width of the distribution, and k_{fm}–the mean value of the rate constant, *i.e.*, the centre of the distribution. The temperature behavior k_{fm} should characterize the mean Arrhenius parameters of the regarded motion in the sample, *i.e.*, the activation barrier and collision factor. So, on a descriptive level, the sample at each temperature will be characterized by three population factors for: (a) static on the ^{2}H NMR time scale phenylene rings ($k_f < 10^3$ Hz << Q_0; $Q_0 = 176 \times 10^3$ Hz); (b) slowly mobile phenyls (10^3 Hz < k_f < 10^7 Hz) and (c) fast moving fragments ($k_f > 10^7$ Hz >> Q_0).

Section S6. Neutron Powder Diffraction Studies

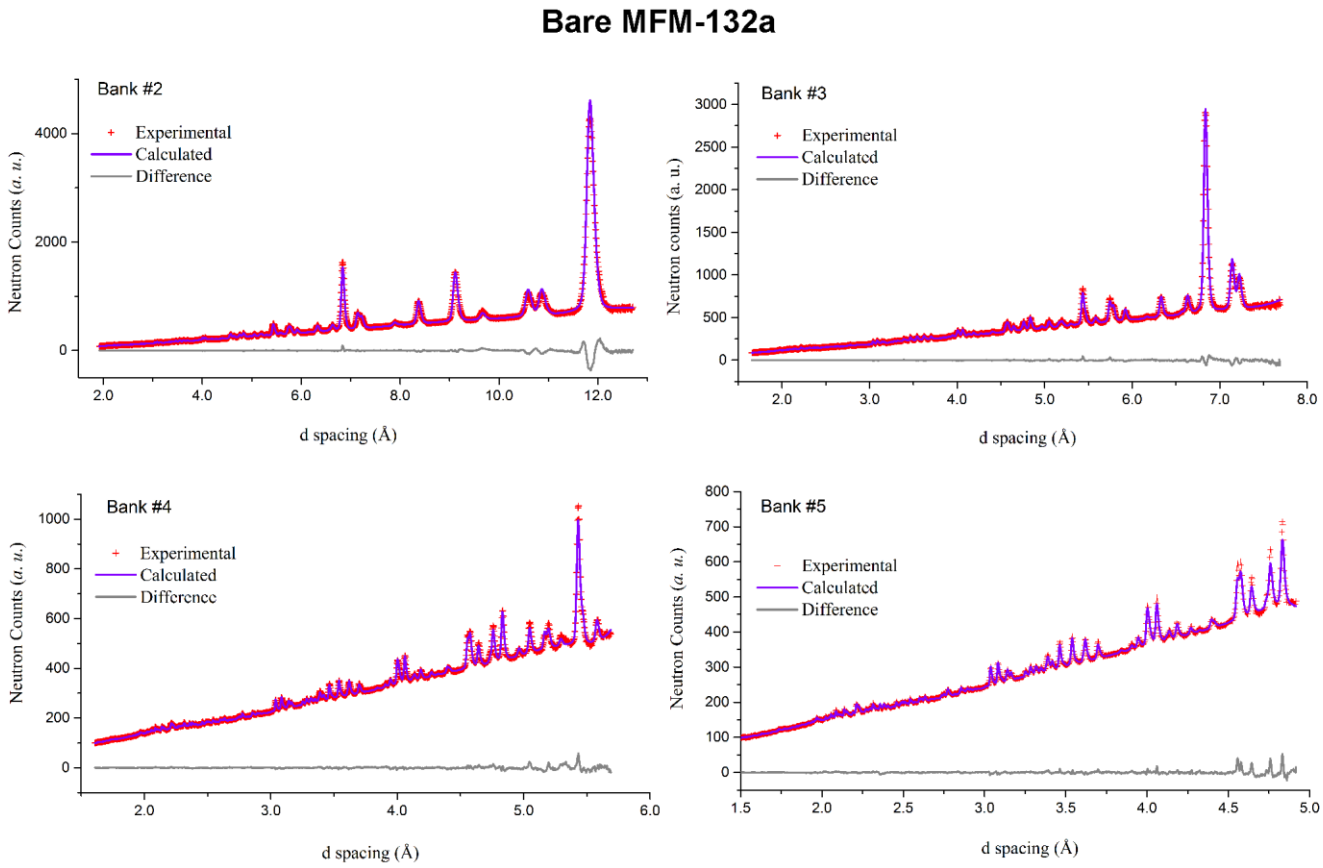

Figure S23. Rietveld refinements of the neutron powder diffraction data collected on different banks for the bare MFM-132a before adsorption of CD_4.

Table S3. Crystallographic parameters of the bare MFM-132a obtained from the Rietveld refinements of the NPD data. [Space group *Fm-3m*, No. 225, a = 47.186(13) Å; CCDC 1499829].

atom	**site**	**x**	**y**	**z**	**occupancy**
Cu1	*48i*	0.3432(2)	0.1568(2)	0	1.0
Cu2	*48i*	0.3796(2)	0.1204(2)	0	1.0
O1	*192l*	0.3246(3)	0.1361(2)	0.0272(3)	1.0
O2	*192l*	0.3586(2)	0.1016(3)	0.0271(3)	1.0
C1	*192l*	0.3363(2)	0.11357(15)	0.03729(19)	1.0
C2	*96k*	0.33418(19)	0.07487(13)	0.07487(13)	1.0
H2A	*96k*	0.3505(2)	0.06529(15)	0.06529(15)	1.0
C3	*192l*	0.32263(18)	0.10009(12)	0.06326(13)	1.0
C4	*192l*	0.29952(15)	0.11370(10)	0.07687(12)	1.0
H4A	*192l*	0.29139(16)	0.13147(14)	0.06869(12)	1.0
C5	*96k*	0.28797(14)	0.10209(10)	0.10209(10)	1.0
C6	*96k*	0.26365(12)	0.11642(9)	0.11642(9)	1.0
C7	*192l*	0.23668(12)	0.11649(8)	0.10312(8)	0.5
C8	*192l*	0.23305(14)	0.10316(9)	0.07641(10)	0.5
H8A	*192l*	0.24949(18)	0.09371(11)	0.06696(12)	0.5
C9	*192l*	0.20608(14)	0.10323(10)	0.06311(11)	0.5
H9A	*192l*	0.20352(17)	0.09384(13)	0.04430(16)	0.5
C10	*192l*	0.18274(13)	0.11664(10)	0.07652(10)	0.5
H10A	*192l*	0.16374(17)	0.11669(11)	0.06715(12)	0.5
C11	*192l*	0.18637(10)	0.12998(8)	0.10323(8)	0.5
H11A	*192l*	0.16993(13)	0.13942(9)	0.11267(10)	0.5
C12	*192l*	0.21334(9)	0.12990(7)	0.11653(7)	0.5
C13	*96k*	0.21697(8)	0.14324(6)	0.14324(6)	1.0
C14	*192l*	0.24395(9)	0.14316(7)	0.15653(7)	0.5
C15	*192l*	0.26729(11)	0.12975(9)	0.14313(8)	0.5
C16	*192l*	0.29426(12)	0.12968(11)	0.15642(10)	0.5
H16A	*192l*	0.31070(16)	0.12023(14)	0.14698(13)	0.5
C17	*192l*	0.29789(13)	0.14301(13)	0.18313(11)	0.5
H17A	*192l*	0.31689(17)	0.14296(15)	0.19250(14)	0.5
C18	*192l*	0.27455(11)	0.15642(11)	0.19654(10)	0.5
H18A	*192l*	0.27711(12)	0.16581(13)	0.21535(15)	0.5
C19	*192l*	0.24758(9)	0.15650(8)	0.18324(8)	0.5
H19A	*192l*	0.23114(13)	0.16594(10)	0.19269(9)	0.5
C20	*96k*	0.19353(5)	0.15670(4)	0.15670(4)	1.0
C21	*96k*	0.18126(4)	0.14443(5)	0.18126(4)	1.0
H21A	*96k*	0.18990(7)	0.12713(11)	0.18990(7)	1.0

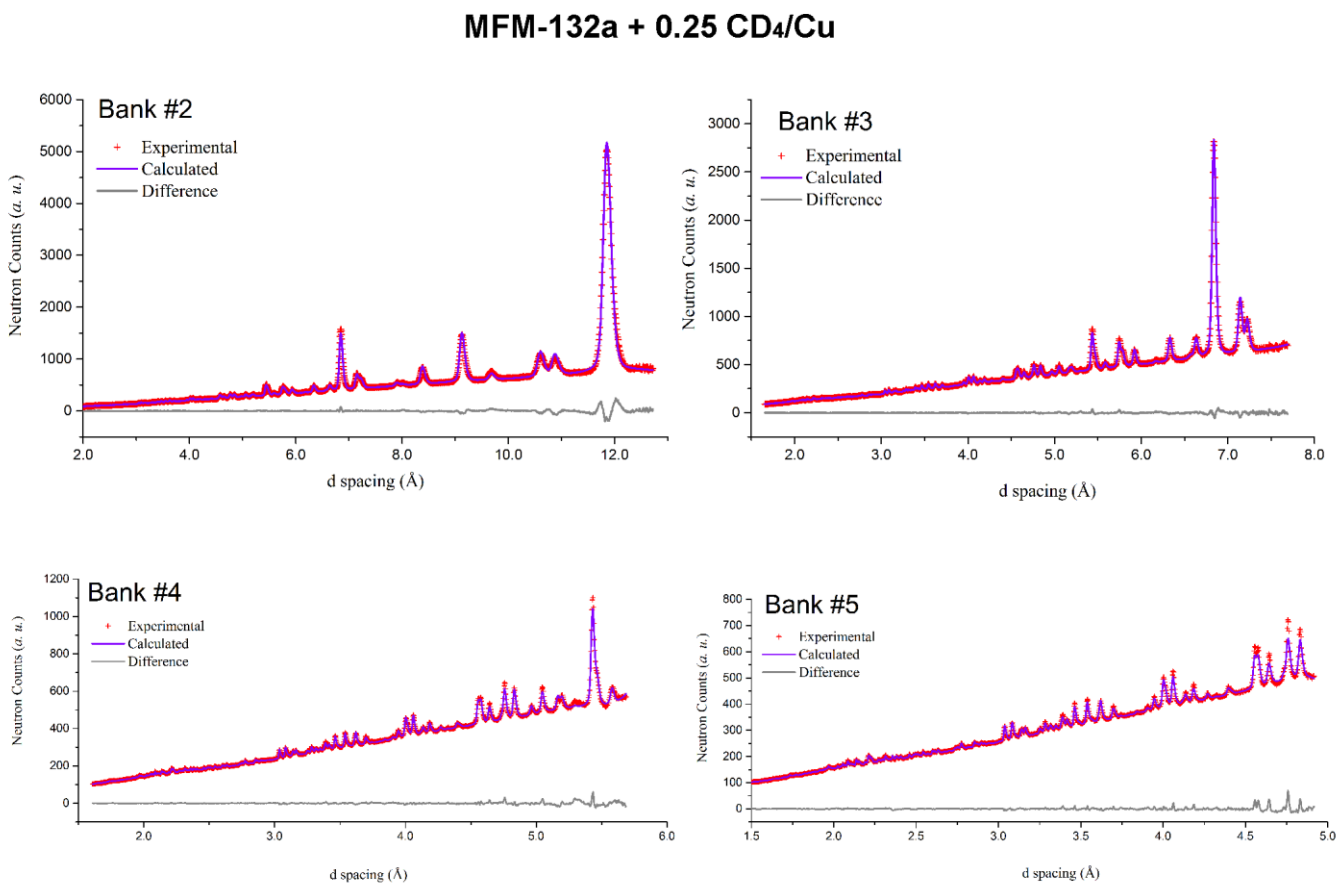

Figure S24. Rietveld refinements of the neutron powder diffraction data for MFM-132a + 0.25 CD_4/Cu.

Table S4. Crystallographic parameters of MFM-132a + 0.25 CD_4/Cu obtained from the Rietveld refinements of the NPD data. [Space group *Fm-3m*, No. 225, a = 47.194(12) Å; CCDC 1499830].

atom	site	x	y	z	occupancy
C1_1 (A1)	*32f*	0.3752(2)	0.3752(2)	0.3752(2)	0.405(7)
D1_1 (A1)	*32f*	0.3879(2)	0.3879(2)	0.3879(2)	0.405(7)
D2_1 (A1)	*96k*	0.3540(2)	0.3795(2)	0.3795(2)	0.202(3)
C1_2 (A2)	*48i*	0.4216(8)	0.0784(8)	0	0.075(5)
D1_2 (A2)	*96k*	0.4164(8)	0.0836(8)	0.02077(18)	0.037(3)
D2_2 (A2)	*48i*	0.4372(8)	0.0628(8)	0	0.075(5)
D3_2 (A2)	*192l*	0.4291(8)	0.0963(8)	-0.01037(9)	0.037(3)
C1_3 (A3)	*48i*	0.3012(7)	0.1988(7)	0	0.075(4)
D1_3 (A3)	*96k*	0.3064(7)	0.1936(7)	0.02077(18)	0.0374(18)
D2_3 (A3)	*48i*	0.2856(7)	0.2144(7)	0	0.075(4)
D3_3 (A3)	*192l*	0.2937(7)	0.1809(7)	-0.01037(9)	0.0374(18)
C1_4 (A4)	*32f*	0.4187(13)	0.4187(13)	0.4187(13)	0.069(6)
D1_4 (A4)	*32f*	0.4315(13)	0.4315(13)	0.4315(13)	0.069(6)
D2_4 (A4)	*96k*	0.4060(13)	0.4060(13)	0.4315(13)	0.034(3)
Cu1	*48i*	0.3434(2)	0.1566(2)	0	1
Cu2	*48i*	0.3797(2)	0.1203(2)	0	1
O1	*192l*	0.3253(3)	0.1356(2)	0.0270(2)	1
O2	*192l*	0.3584(2)	0.1019(3)	0.0277(2)	1
C1	*192l*	0.3360(2)	0.11323(15)	0.03822(18)	1
C2	*96k*	0.33371(19)	0.07515(14)	0.07515(14)	1
H2A	*96k*	0.3500(2)	0.06557(16)	0.06557(16)	1
C3	*192l*	0.32223(18)	0.10019(12)	0.06362(14)	1
C4	*192l*	0.29928(16)	0.11370(10)	0.07713(12)	1
H4A	*192l*	0.29114(16)	0.13147(15)	0.06895(13)	1
C5	*96k*	0.28781(15)	0.10217(10)	0.10217(10)	1
C6	*96k*	0.26343(12)	0.11652(9)	0.11652(9)	1
C7	*192l*	0.23671(12)	0.11675(8)	0.10320(8)	0.5
C8	*192l*	0.23318(14)	0.10369(9)	0.07658(10)	0.5
H8A	*192l*	0.24964(18)	0.09426(12)	0.06715(12)	0.5
C9	*192l*	0.20646(15)	0.10392(10)	0.06325(11)	0.5
H9A	*192l*	0.20396(17)	0.09465(13)	0.04437(16)	0.5
C10	*192l*	0.18326(13)	0.11722(10)	0.07655(10)	0.5
H10A	*192l*	0.16430(18)	0.11738(11)	0.06710(12)	0.5
C11	*192l*	0.18678(10)	0.13028(8)	0.10317(8)	0.5
H11A	*192*	0.17033(14)	0.13971(10)	0.11260(10)	0.5
C12	*192l*	0.21351(10)	0.13005(7)	0.11649(7)	0.5
C13	*96k*	0.21704(8)	0.14312(6)	0.14312(6)	1
C14	*192l*	0.24376(9)	0.14288(7)	0.15644(7)	0.5
C15	*192l*	0.26696(11)	0.12959(9)	0.14314(8)	0.5
C16	*192l*	0.29368(12)	0.12936(11)	0.15647(10)	0.5
H16A	*192l*	0.31014(16)	0.11992(14)	0.14703(13)	0.5
C17	*192l*	0.29721(13)	0.14242(13)	0.18309(11)	0.5
H17A	*192l*	0.31616(17)	0.14226(15)	0.19254(14)	0.5
C18	*192l*	0.27401(11)	0.15572(11)	0.19638(10)	0.5
H18A	*192l*	0.27651(12)	0.16498(14)	0.21526(16)	0.5
C19	*192l*	0.24729(10)	0.15595(9)	0.18306(8)	0.5
H19A	*192l*	0.23083(14)	0.16538(10)	0.19249(9)	0.5
C20	*96k*	0.19330(5)	0.15672(4)	0.15672(4)	1
C21	*96k*	0.18110(4)	0.14453(5)	0.18110(4)	1
H21A	*96k*	0.18975(7)	0.12724(12)	0.18975(7)	1

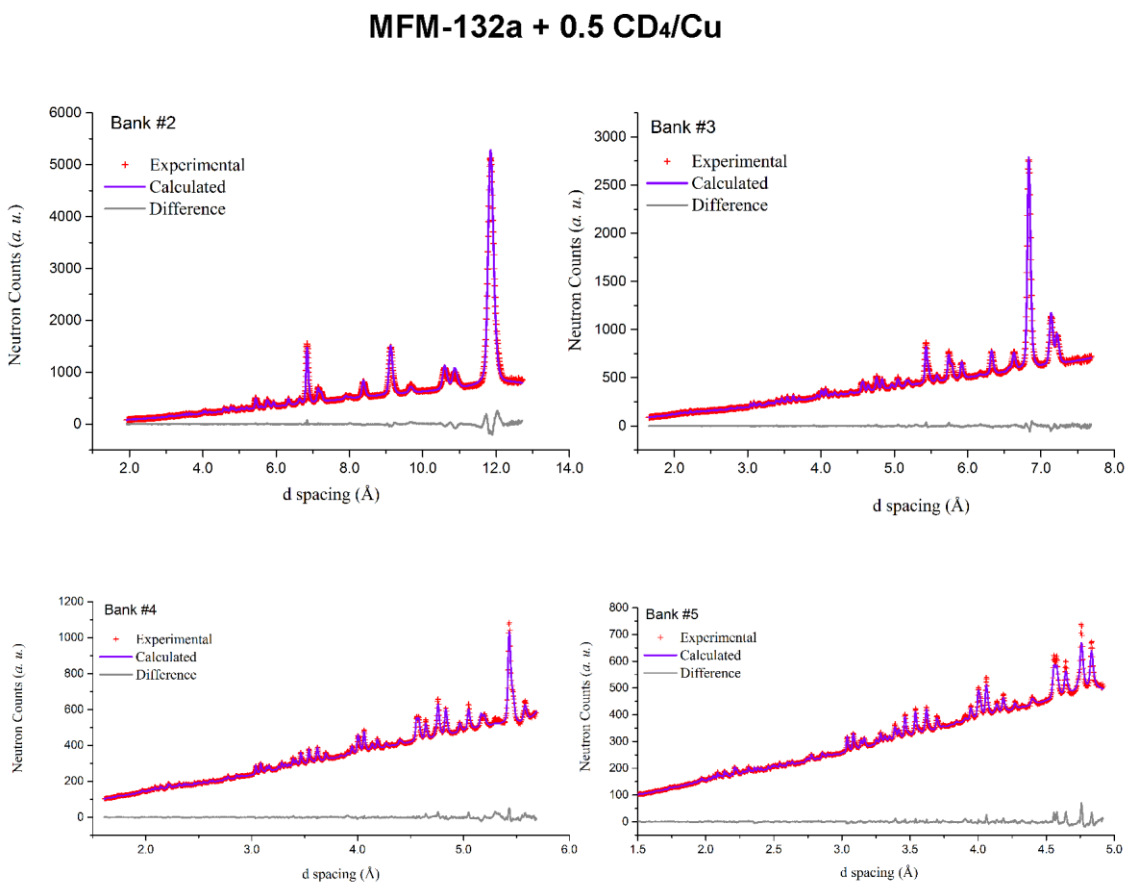

Figure S25. Rietveld refinements of the neutron powder diffraction data for MFM-132a + 0.5 CD_4/Cu.

Table S5. Crystallographic parameters of MFM-132a + 0.5 CD_4/Cu obtained from the Rietveld refinements of the NPD data. [Space group *Fm-3m*, No. 225, a = 47.199(12) Å; CCDC 1499831].

atom	site	x	y	z	occupancy
C1_1 (A1)	*32f*	0.3698(2)	0.3698(2)	0.3698(2)	0.639(9)
D1_1 (A1)	*32f*	0.3825(2)	0.3825(2)	0.3825(2)	0.639(9)
D2_1 (A1)	*96k*	0.3486(2)	0.3741(2)	0.3741(2)	0.1065(15)
C1_2 (A2)	*48i*	0.4212(5)	0.0788(5)	0	0.170(7)
D1_2 (A2)	*96k*	0.4160(5)	0.0840(5)	0.02077(18)	0.085(4)
D2_2 (A2)	*48i*	0.4368(5)	0.0632(5)	0	0.170(7)
D3_2 (A2)	*192l*	0.4287(5)	0.0967(5)	-0.01037(9)	0.085(4)
C1_3 (A3)	*48i*	0.3018(5)	0.1982(5)	0	0.129(4)
D1_3 (A3)	*96k*	0.3070(5)	0.1930(5)	0.02077(18)	0.065(2)
D2_3 (A3)	*48i*	0.2863(5)	0.2137(5)	0	0.129(4)
D3_3 (A3)	*192l*	0.2943(5)	0.1802(5)	-0.01037(9)	0.065(2)
C1_4 (A4)	*32f*	0.4123(6)	0.4123(6)	0.4123(6)	0.215(8)
D1_4 (A4)	*32f*	0.4251(6)	0.4251(6)	0.4251(6)	0.215(8)
D2_4 (A4)	*96k*	0.3996(6)	0.3996(6)	0.4251(6)	0.0359(14)
Cu1	*48i*	0.3438(2)	0.1562(2)	0	1
Cu2	*48i*	0.3793(2)	0.1207(2)	0	1
O1	*192l*	0.3250(3)	0.1353(2)	0.0271(2)	1
O2	*192l*	0.3585(2)	0.1021(3)	0.0281(2)	1
C1	*192l*	0.3361(2)	0.11332(16)	0.03801(18)	1
C2	*96k*	0.3336(2)	0.07509(14)	0.07509(14)	1
H2A	*96k*	0.3500(2)	0.06544(17)	0.06544(17)	1
C3	*192l*	0.32214(19)	0.10006(13)	0.06358(14)	1
C4	*192l*	0.29923(16)	0.11352(11)	0.07704(12)	1
H4A	*192l*	0.29102(17)	0.13141(15)	0.06879(13)	1
C5	*96k*	0.28778(15)	0.10201(11)	0.10201(11)	1
C6	*96k*	0.26306(13)	0.11653(9)	0.11653(9)	1
C7	*192l*	0.23647(12)	0.11689(8)	0.10313(9)	0.5
C8	*192l*	0.23304(14)	0.10401(10)	0.07649(10)	0.5
H8A	*192l*	0.24965(19)	0.09452(12)	0.06701(13)	0.5
C9	*192l*	0.20645(15)	0.10436(11)	0.06309(11)	0.5
H9A	*192l*	0.20399(17)	0.09513(13)	0.04400(17)	0.5
C10	*192l*	0.18328(13)	0.11759(10)	0.07632(10)	0.5
H10A	*192l*	0.16422(18)	0.11785(12)	0.06671(13)	0.5
C11	*192l*	0.18670(11)	0.13047(8)	0.10295(8)	0.5
H11A	*192l*	0.17010(14)	0.13995(10)	0.11244(10)	0.5
C12	*192l*	0.21329(10)	0.13012(7)	0.11636(7)	0.5
C13	*96k*	0.21672(9)	0.14299(6)	0.14299(6)	1
C14	*192l*	0.24331(9)	0.14264(8)	0.15640(7)	0.5
C15	*192l*	0.26648(11)	0.12941(9)	0.14317(9)	0.5
C16	*192l*	0.29308(13)	0.12906(12)	0.15657(11)	0.5
H16A	*192l*	0.30968(17)	0.11957(14)	0.14709(13)	0.5
C17	*192l*	0.29650(13)	0.14193(13)	0.18321(12)	0.5
H17A	*192l*	0.31556(18)	0.14168(15)	0.19281(14)	0.5
C18	*192l*	0.27333(12)	0.15517(12)	0.19644(10)	0.5
H18A	*192l*	0.27578(13)	0.16439(14)	0.21553(16)	0.5
C19	*192l*	0.24674(10)	0.15552(9)	0.18304(8)	0.5
H19A	*192l*	0.23013(15)	0.16500(10)	0.19252(10)	0.5
C20	*96k*	0.19301(5)	0.15653(5)	0.15653(5)	1
C21	*96k*	0.18085(5)	0.14437(5)	0.18085(5)	1
H21A	*96k*	0.18957(7)	0.12695(12)	0.18957(7)	1

Table S6. Unit cell parameters for MFM-132a determined by Rietveld refinements for each CD_4 gas loading and goodness of fit.

CD_4 dosage per Cu	lattice parameter (Å)	+ background		GoF
		wR_p (%)	R_p (%)	
0 (bare)	47.186(13)	0.77	1.28	3.01
0.25	47.194(12)	0.73	1.21	2.91
0.5	47.199(12)	0.82	1.26	3.24

NPD for CD_4-loaded MFM-115a

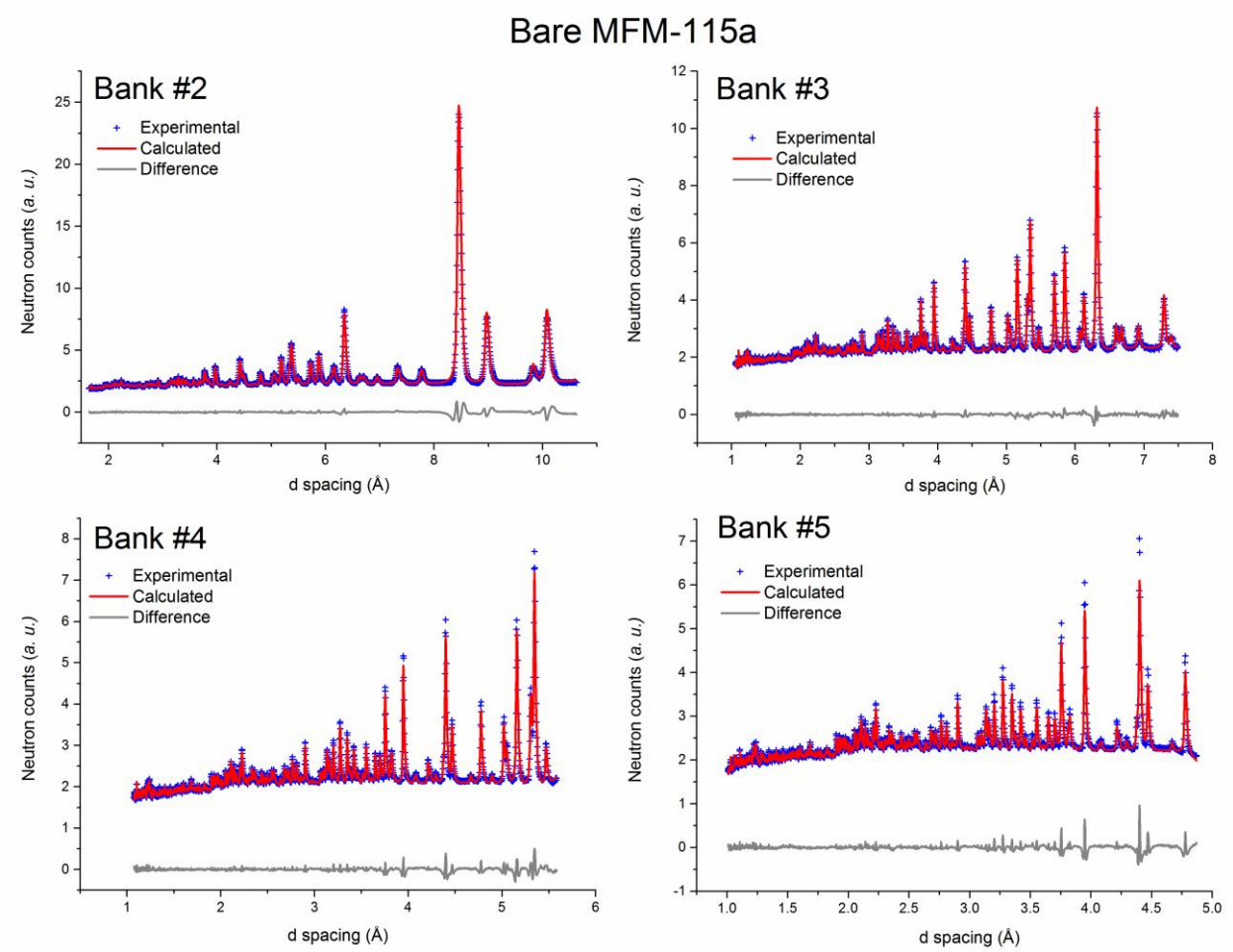

Figure S26. Rietveld refinements of the neutron powder diffraction data collected on different banks for the bare MFM-115a before adsorption of CD_4.

Table S7. Crystallographic parameters of bare MFM-115a obtained from the Rietveld refinements of the NPD data. [Space group *Fm-3m*, No. 225, a = 43.669(4) Å; CCDC 1499826].

atom	site	x	y	z	occupancy
Cu1	*48i*	0.17033(10)	0	0.17033(10)	1
Cu2	*48i*	0.13039(11)	0	0.13039(11)	1
O1	*192l*	0.14625(16)	0.0314(2)	0.1902(2)	1
O2	*192l*	0.11008(18)	0.0318(2)	0.15391(18)	1
C1	*192l*	0.12222(13)	0.04140(16)	0.17810(16)	1
C2	*192l*	0.10655(12)	0.06714(14)	0.19395(15)	1
C3	*96k*	0.08089(13)	0.08089(13)	0.18021(16)	1
H3A	*96k*	0.07191(14)	0.07191(14)	0.15941(18)	1
C4	*192l*	0.11842(11)	0.07902(13)	0.22142(13)	1
H4A	*192l*	0.13784(12)	0.06858(13)	0.23182(13)	1
C5	*96k*	0.10464(10)	0.10464(10)	0.23516(12)	1
C6	*96k*	0.11710(10)	0.11710(10)	0.26399(10)	1
C7	*192l*	0.14902(9)	0.11877(12)	0.26789(9)	0.5
H7A	*192l*	0.16387(12)	0.11070(16)	0.25033(12)	0.5
C8	*192l*	0.16132(7)	0.13106(10)	0.29499(8)	0.5
H8A	*192l*	0.18548(11)	0.13229(12)	0.29795(9)	0.5
C9	*192l*	0.09748(9)	0.12779(11)	0.28719(9)	0.5
H9A	*192l*	0.07332(12)	0.12655(13)	0.28424(11)	0.5
C10	*192l*	0.10978(7)	0.14008(8)	0.31429(8)	0.5
H10A	*192l*	0.09493(8)	0.14814(11)	0.33186(11)	0.5
C11	*96k*	0.14170(6)	0.14170(6)	0.31819(7)	1
N1	*32f*	0.15422(5)	0.15422(5)	0.34578(5)	1

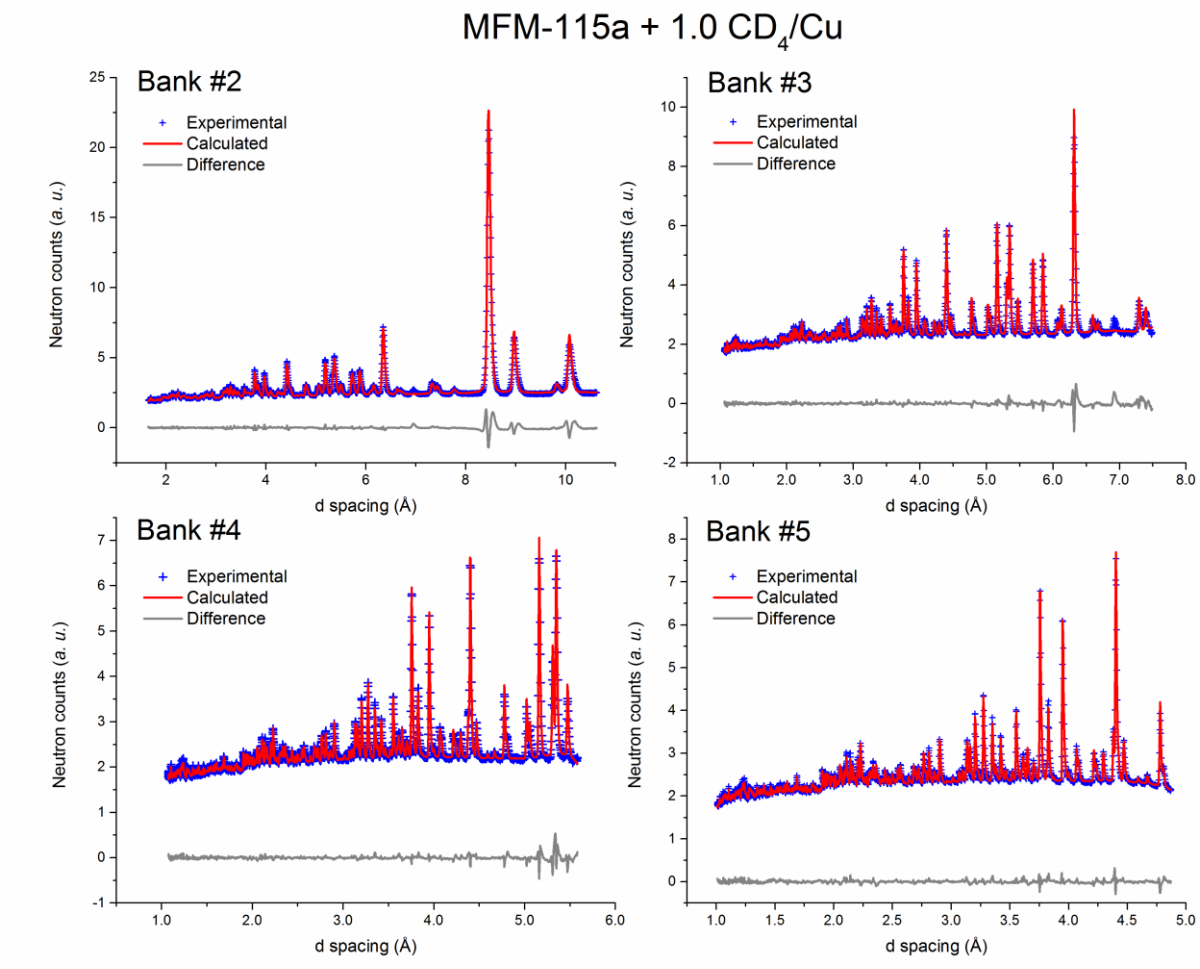

Figure S27. Rietveld refinements of the neutron powder diffraction data for MFM-115a + 1.0 CD_4/Cu.

Table S8. Crystallographic parameters of MFM-115a + 1.0 CD_4/Cu obtained from the Rietveld refinements of the NPD data. [Space group *Fm-3m*, No. 225, a = 43.692(11) Å; CCDC 1499827].

atom	site	x	y	z	occupancy
C1_1 (A1')	*32f*	0.10508(15)	0.10508(15)	0.10508(15)	1.000(14)
D1_1 (A1')	*32f*	0.09134(15)	0.09134(15)	0.09134(15)	1.000(14)
D2_1 (A1')	*96k*	0.10049(15)	0.10049(15)	0.12798(15)	0.333(5)
C1_2 (A2')	*32f*	0.1502(6)	0.1502(6)	0.1502(6)	0.256(15)
D1_2 (A2')	*32f*	0.1364(6)	0.1364(6)	0.1364(6)	0.256(15)
D2_2 (A2')	*96k*	0.1456(6)	0.1456(6)	0.1731(6)	0.085(5)
C1_3 (A3')	*48i*	0.0839(2)	0.0839(2)	0	0.357(4)
D1_3 (A3')	*48i*	0.0671(2)	0.0671(2)	0	0.357(4)
D2_3 (A3')	*192l*	0.0742(2)	0.1049(2)	-0.00580(5)	0.0892(10)
D3_3 (A3')	*192l*	0.1008(2)	0.0783(2)	-0.01587(13)	0.0892(10)
D4_3 (A3')	*192l*	0.0936(2)	0.0854(2)	0.02167(18)	0.0892(10)
C1_4 (A4')	*48i*	0.2180(8)	0.2180(8)	0	0.071(3)
D1_4 (A4')	*48i*	0.2348(8)	0.2348(8)	0	0.071(3)
D2_4 (A4')	*192l*	0.2277(8)	0.1971(8)	-0.00580(5)	0.0177(7)
D3_4 (A4')	*192l*	0.2012(8)	0.2236(8)	-0.01587(13)	0.0177(7)
D4_4 (A4')	*192l*	0.2083(8)	0.2165(8)	0.02167(18)	0.0177(7)
Cu1	*48i*	0.17062(12)	0	0.17062(12)	1
Cu2	*48i*	0.13200(12)	0	0.13200(12)	1
O1	*192l*	0.14548(19)	0.0306(2)	0.1909(3)	1
O2	*192l*	0.1111(2)	0.0320(2)	0.1544(2)	1
C1	*192l*	0.12211(16)	0.0415(2)	0.1788(2)	1
C2	*192l*	0.10660(15)	0.06715(18)	0.1944(2)	1
C3	*96k*	0.08112(16)	0.08112(16)	0.1811(2)	1
H3	*96k*	0.07159(18)	0.07159(18)	0.1602(2)	1
C4	*192l*	0.11873(13)	0.07929(16)	0.22107(17)	1
H4A	*192l*	0.13873(16)	0.06882(17)	0.23153(18)	1
C5	*96k*	0.10539(13)	0.10539(13)	0.23439(16)	1
C6	*96k*	0.11876(12)	0.11876(12)	0.26372(13)	1
C7	*192l*	0.15018(11)	0.12017(15)	0.26729(12)	0.5
H7A	*192l*	0.16530(15)	0.11207(19)	0.24927(16)	0.5
C8	*192l*	0.16234(9)	0.13254(12)	0.29382(10)	0.5
H8A	*192l*	0.18701(14)	0.13415(15)	0.29662(11)	0.5
C9	*192l*	0.09949(11)	0.12845(13)	0.28667(12)	0.5
H9A	*192l*	0.07482(15)	0.12684(16)	0.28387(14)	0.5
C10	*192l*	0.11165(9)	0.14081(10)	0.31319(10)	0.5
H10A	*192l*	0.09653(10)	0.14892(14)	0.33121(14)	0.5
C11	*96k*	0.14307(8)	0.14307(8)	0.31677(9)	1
N1	*32f*	0.15570(6)	0.15570(6)	0.34430(6)	1

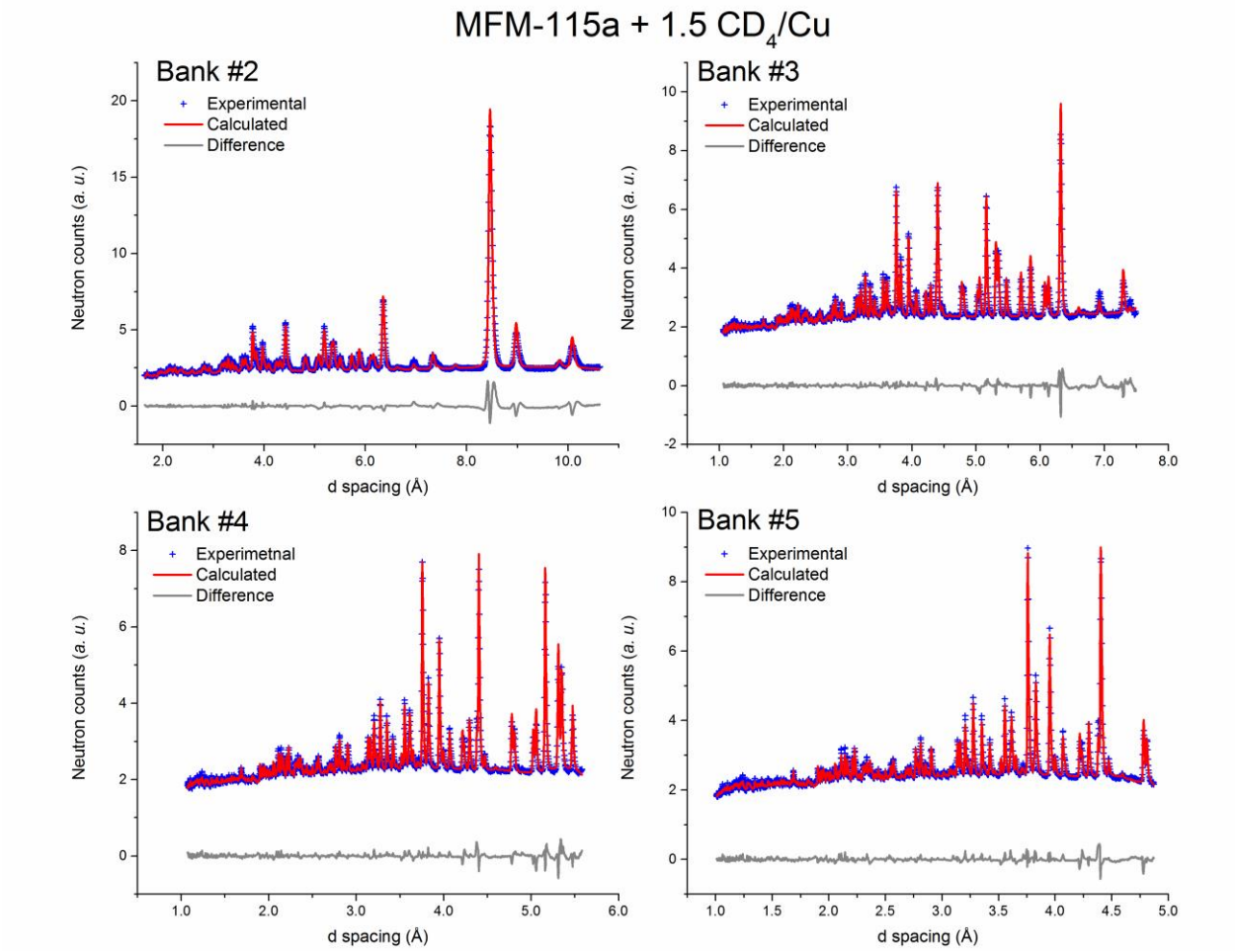

Figure S28. Rietveld refinements of the neutron powder diffraction data for MFM-115a + 1.5 CD_4/Cu.

Table S9. Crystallographic parameters of MFM-115a + 1.5 CD_4/Cu obtained from the Rietveld refinements of the NPD data. [Space group *Fm-3m*, No. 225, a = 43.709(19) Å; CCDC 1499828].

atom	**site**	**x**	**y**	**z**	**occupancy**
C1_1(A1')	*32f*	0.09853(16)	0.09853(16)	0.09853(16)	1.000(16)
D1_1(A1')	*32f*	0.08479(16)	0.08479(16)	0.08479(16)	1.000(16)
D2_1(A1')	*96k*	0.09394(16)	0.09394(16)	0.12142(16)	0.333(5)
C1_2(A2')	*32f*	0.1439(2)	0.1439(2)	0.1439(2)	0.99(2)
D1_2(A2')	*32f*	0.1302(2)	0.1302(2)	0.1302(2)	0.99(2)
D2_2(A2')	*96k*	0.1394(2)	0.1394(2)	0.1668(2)	0.331(8)
C1_3(A3')	*48i*	0.0841(3)	0.0841(3)	0	0.818(7)
D1_3(A3')	*48i*	0.0673(3)	0.0673(3)	0	0.818(7)
D2_3(A3')	*192l*	0.0744(3)	0.1051(3)	-0.0058057(8)	0.2045(17)
D3_3(A3')	*192l*	0.1010(3)	0.0785(3)	-0.015861(2)	0.2045(17)
D4_3(A3')	*192l*	0.0938(3)	0.0856(3)	0.021667(3)	0.2045(17)
C1_4(A4')	*48i*	0.2178(6)	0.2178(6)	0	0.140(4)
D1_4(A4')	*48i*	0.2346(6)	0.2346(6)	0	0.140(4)
D2_4(A4')	*192l*	0.2275(6)	0.1968(6)	-0.0058057(8)	0.0350(10)
D3_4(A4')	*192l*	0.2009(6)	0.2234(6)	-0.015861(2)	0.0350(10)
D4_4(A4')	*192l*	0.2080(6)	0.2163(6)	0.021667(3)	0.0350(10)
Cu1	*48i*	0.17083(19)	0	0.17083(19)	1
Cu2	*48i*	0.1333(2)	0	0.1333(2)	1
O1	*192l*	0.1449(3)	0.0300(4)	0.1912(4)	1
O2	*192l*	0.1119(4)	0.0320(4)	0.1554(4)	1
C1	*192l*	0.1228(3)	0.0405(3)	0.1790(4)	1
C2	*192l*	0.1069(2)	0.0672(3)	0.1950(3)	1
C3	*96k*	0.0813(3)	0.0813(3)	0.1820(4)	1
H3A	*96k*	0.0717(3)	0.0717(3)	0.1618(4)	1
C4	*192l*	0.1195(2)	0.0797(3)	0.2211(3)	1
H4A	*192l*	0.1393(3)	0.0697(3)	0.2312(3)	1
C5	*96k*	0.1065(2)	0.1065(2)	0.2342(3)	1
C6	*96k*	0.1204(2)	0.1204(2)	0.2632(2)	1
C7	*192l*	0.15176(19)	0.1218(2)	0.2661(2)	0.5
H7A	*192l*	0.1663(2)	0.1137(3)	0.2483(3)	0.5
C8	*192l*	0.16427(15)	0.13463(19)	0.29203(17)	0.5
H8A	*192l*	0.1884(2)	0.1365(2)	0.29425(19)	0.5
C9	*192l*	0.10158(18)	0.1297(2)	0.2863(2)	0.5
H9A	*192l*	0.0774(3)	0.1278(3)	0.2840(2)	0.5
C10	*192l*	0.11409(14)	0.14261(17)	0.31224(17)	0.5
H10A	*192l*	0.09956(18)	0.1506(2)	0.3300(2)	0.5
C11	*96k*	0.14543(12)	0.14543(12)	0.31512(15)	1
N1	*32f*	0.15825(10)	0.15825(10)	0.34175(10)	1

Table S10. Unit cell parameters for MFM-115a determined from Rietveld refinements for the bare sample and the samples with CD_4 loading and goodness of fit.

CD_4 dosage per Cu	lattice parameter (Å)	+ background		GoF
		wR_p (%)	R_p (%)	
0 (bare)	43.669(4)	1.37	1.30	4.51
1.0	43.692(11)	1.56	1.37	5.29
1.5	43.709(19)	1.59	1.39	5.39

References

1. Huang, H.; Fu, Q.; Zhuang, S.; Liu, Y.; Wang, L.; Chen, J.; Ma, D.; Yang, C. *J. Phys. Chem. C* **2011**, *115*, 4872–4878.

2. Winter, G. *J. Appl. Cryst.* **2010**, *43*, 186–190.

3. Sheldrick, G. M. *Acta Cryst. Sect. C* **2015**, *71*, 3−8.

4. Spek, A. L. *Acta Cryst. Sect. C* **2015**, *71*, 9–18.

5. Yan, Y.; Lin, X.; Yang, S.; Blake, A. J.; Dailly, A.; Champness, N. R.; Hubberstey, P.; Schröder, M. *Chem. Comm.* **2009**, 1025–1027.

6. Yan, Y.; Yang, S.; Blake, A. J.; Lewis, W.; Poirier, E.; Barnett, S. A.; Champness, N. R.; Schröder, M. *Chem. Comm.* **2011**, *47*, 9995–9997.

7. Thompson, S. P.; Parker, J. E.; Potter, J.; Hill, T. P.; Birt, A.; Cobb, T. M.; Yuan, F.; Tang, C. C. *Rev. Sci. Instrum.* **2009**, *80*, 075107.

8. Czepirski, L.; Jagiełło, J. *Chem. Eng. Sci*. **1989,** 44, 797–801.

9. Hu, Z.-G.; Liu, J.; Li, G. A.; Dong, Z. B. *J. Chem. Res. (S)* **2003**, *12*, 778–779.

10. Goodbrand, H. B.; Hu, N.-X. *J. Org. Chem.* **1999**, *64*, 670–674.

11. Jelinski, L. W. Deuterium NMR of Solid Polymers. in *High resolution NMR spectroscopy of synthetic polymers in bulk*; Komoroski, R. A., Ed.; VCH Publishers: New York, **1986**; Vol. 7, p. 335.

12. Abragam, A. The Principles of Nuclear Magnetism; Oxford University Press, **1961**.

13. Spiess, H. W. NMR Basic Principles and Progress; Springer-Verlag, New York, **1978**, Vol. 15, p. 55.

14. Wittebort, R. J.; Szabo, A. *J. Chem. Phys.* **1978**, *69*, 1722.

15. Wittebort, R. J.; Olejniczak, E. T.; Griffin, R. G. *J. Chem. Phys.* **1987**, *86* (10), 5411.

16. Lipari, G.; Szabo, A. *Biophys. J.* **1980**, *30*, 489.

17. Schwartz, L. J.; Meirovitch, E.; Ripmeester, J. A.; Freed, J. H. *J. Phys. Chem.* **1983**, *87*, 4453.